



HAL
open science

Cytochrome c prompts the recruitment of its nuclear partners SET/TAF- $I\beta$ and NPM1 into biomolecular condensates

Miguel Á. Casado-Combreras, Adrián Velázquez-Campoy, Marlène Martinho, Valérie Belle, Miguel A de la Rosa, Irene Díaz-Moreno

► **To cite this version:**

Miguel Á. Casado-Combreras, Adrián Velázquez-Campoy, Marlène Martinho, Valérie Belle, Miguel A de la Rosa, et al.. Cytochrome c prompts the recruitment of its nuclear partners SET/TAF- $I\beta$ and NPM1 into biomolecular condensates. *iScience*, 2024, pp.110435. 10.1016/j.isci.2024.110435 . hal-04636008

HAL Id: hal-04636008

<https://hal.science/hal-04636008>

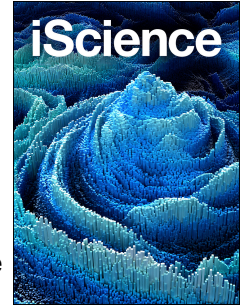
Submitted on 5 Jul 2024

HAL is a multi-disciplinary open access archive for the deposit and dissemination of scientific research documents, whether they are published or not. The documents may come from teaching and research institutions in France or abroad, or from public or private research centers.

L'archive ouverte pluridisciplinaire **HAL**, est destinée au dépôt et à la diffusion de documents scientifiques de niveau recherche, publiés ou non, émanant des établissements d'enseignement et de recherche français ou étrangers, des laboratoires publics ou privés.

Copyright

Journal Pre-proof



Cytochrome *c* prompts the recruitment of its nuclear partners SET/TAF- β and NPM1 into biomolecular condensates

Miguel Á. Casado-Combreras, Adrián Velázquez-Campoy, Marlène Martinho, Valérie Belle, Miguel A. De la Rosa, Irene Díaz-Moreno

PII: S2589-0042(24)01660-2

DOI: <https://doi.org/10.1016/j.isci.2024.110435>

Reference: ISCI 110435

To appear in: *ISCIENCE*

Received Date: 11 March 2024

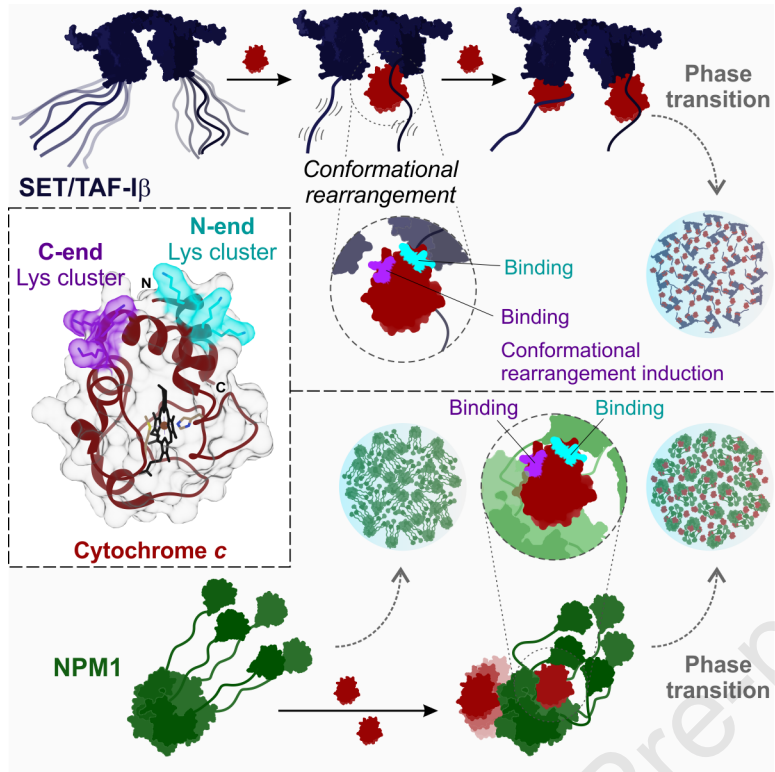
Revised Date: 16 May 2024

Accepted Date: 28 June 2024

Please cite this article as: Casado-Combreras, M.Á., Velázquez-Campoy, A., Martinho, M., Belle, V., De la Rosa, M.A., Díaz-Moreno, I., Cytochrome *c* prompts the recruitment of its nuclear partners SET/TAF- β and NPM1 into biomolecular condensates, *ISCIENCE* (2024), doi: <https://doi.org/10.1016/j.isci.2024.110435>.

This is a PDF file of an article that has undergone enhancements after acceptance, such as the addition of a cover page and metadata, and formatting for readability, but it is not yet the definitive version of record. This version will undergo additional copyediting, typesetting and review before it is published in its final form, but we are providing this version to give early visibility of the article. Please note that, during the production process, errors may be discovered which could affect the content, and all legal disclaimers that apply to the journal pertain.

© 2024 Published by Elsevier Inc.



1 **Cytochrome c prompts the recruitment of its nuclear partners SET/TAF-I β**
2 **and NPM1 into biomolecular condensates**

Miguel Á. Casado-Combreras¹, Adrián Velázquez-Campoy²⁻⁵, Marlène Martinho⁶,
Valérie Belle⁶, Miguel A. De la Rosa¹, Irene Díaz-Moreno^{1,*}

¹Institute for Chemical Research (IIQ), Scientific Research Center “Isla de la Cartuja” (cicCartuja), University of Seville - CSIC, Seville, Spain.

²Institute for Biocomputation and Physic of Complex Systems (BIFI), Joint Unit GBsC-CSIC-BIFI, University of Zaragoza, Zaragoza, Spain.

³Departament of Biochemistry and Molecular and Cellular Biology, University of Zaragoza, Zaragoza, Spain.

⁴Institute for Health Research Aragón (IIS Aragón), Zaragoza, Spain.

⁵Centre for Biomedical Research Network of Hepatic and Digestive Diseases (CIBERehd), Madrid, Spain.

⁶Aix Marseille Univ, CNRS, BIP, Bioénergétique et Ingénierie des Protéines, IMM, IM2B, Marseille, France.

*Corresponding author. E-mail address: idadiazmoreno@us.es (I. Díaz-Moreno)

Summary

3 Compartmentalization of proteins by liquid-liquid phase separation (LLPS) is used by
4 cells to control biochemical reactions spatially and temporally. Among them, the
5 recruitment of proteins to DNA foci and nucleolar trafficking occurs by biomolecular
6 condensation. Within this frame, the oncoprotein SET/TAF-I β plays a key role in both
7 chromatin remodeling and DNA damage response, as does nucleophosmin (NPM1)
8 which indeed participates in nucleolar ribosome synthesis. Whereas phase separation
9 by NPM1 is widely characterized, little is known about that undergone by SET/TAF-I β .
10 Here, we show that SET/TAF-I β experiences phase transition together with respiratory
11 cytochrome *c* (Cc), which translocates to the nucleus upon DNA damage. Here we
12 report the molecular mechanisms governing Cc-induced phase separation of SET/TAF-
13 I β and NPM1, where two lysine-rich clusters of Cc are essential to recognize molecular
14 surfaces on both partners in a specific and coordinated manner. Cc thus emerges as a
15 small, globular protein with sequence-encoded heterotypic phase-separation
16 properties.

17

18 **Keywords:** Biomolecular condensates, cytochrome *c*, liquid-liquid phase separation,
19 nucleophosmin (NPM1), SET/TAF-I β

20

21 Introduction

22 Biomolecular condensates have attracted a wealth of research interest in recent years
23 as an important physiological phenomenon for the spatial-temporal regulation of many
24 biochemical processes¹. Such biomolecular condensates are supramolecular, micron-
25 sized structures formed by proteins and often nucleic acids that reorganize from a
26 diluted into a—usually liquid-like—dense phase, through a process known as liquid-
27 liquid phase separation (LLPS)^{1,2}. Condensates lead the enrichment or exclusion of
28 certain macromolecules, favoring or restricting different biochemical events^{3–5}. Indeed,
29 LLPS is the primary basis for the formation of membraneless organelles (MLOs)—such
30 as nucleoli, P-granules or nuclear speckles and paraspeckles^{6–8}—as well as other
31 transient compartments—including DNA damage foci or stress granules^{3,9–11}.

32 The formation of biomolecular condensates requires the onset of multivalent
33 interactions, established by proteins which usually are multi-domain or contain
34 intrinsically disordered regions (IDRs)^{3,12}. Such interactions encompass weak physical
35 crosslinks, including electrostatic forces, π - π stacking, cation- π , hydrophobic
36 interactions or hydrogen bonds (H-bonds) formation^{13–17}. In particular, when the
37 attraction between two macromolecules is based on electrostatic complementarity, they
38 can undergo spontaneous phase transitions that are known as electrostatic complex
39 coacervation^{18,19}. The driving forces for such kind of phase transitions actually consist
40 of long-range electrostatic interactions driving the association between oppositely
41 charged macromolecules, along with counterion release²⁰. Therefore, electrostatic
42 coacervates are dissolved at high ionic strength²¹. Usually, complex coacervation gives
43 rise to short-range interactions that stabilize LLPS or trigger other processes such as
44 percolation or gelation^{19,20}. Currently, the distinction between LLPS and other
45 percolation processes that can be coupled to it, such as gelation or solid-transitions, is
46 well established based on the viscoelastic and dynamic properties of condensates. The
47 term phase separation (PS) will then more accurately refer to condensation processes
48 in a general manner²².

49
50 In proteins, residues capable of forming such associations are often distributed within
51 patches or sequence repeats that confer site-specific associativity to the protein²³.
52 Such interacting motifs—or even particular residues—are known as “stickers” and are
53 interspersed with non-interacting residues or “spacers”^{20,24}. While stickers essentially
54 determine the type and strength of interactions that can be established^{20,25}, spacers are
55 critical in determining the conformational landscape, orientation and availability of
56 stickers in the case of both IDRs or intrinsically folded domains and globular proteins²⁶.
57 Specific sticker distributions and sequence features—usually referred to as “molecular
58 grammars”—have been profoundly investigated to establish the molecular tenets of
59 PS, especially for IDRs^{14,19,20,27–29}. Although proteins with a defined folding are rarely
60 involved in LLPS processes³⁰, featuring sticker patches with specific orientations
61 provides them multivalency and then, the ability to undergo phase separation^{26,31}. This
62 is the case of cytochrome *c* (Cc), a small and globular lysine-rich polypeptide which
63 exemplifies the kind of particles described above.

64
65 Cc is a small globular heme protein that is translocated from the mitochondria to the
66 nucleus under conditions of DNA damage and participates in the stress response
67 through a network of interactions^{32,33}. Soon after DNA injury, Cc is capable to be

68 integrated into the nucleolus and interact with nucleophosmin (NPM1), which is an
69 abundant nucleolar protein involved in ribosome biogenesis. Then, Cc displaces the
70 alternative reading frame (ARF) tumor suppressor out of the nucleolus, which in turn
71 prevents proteasomal degradation of p53 by sequestering human double-minute 2
72 protein (HDM2)^{34,35}. Nuclear Cc has also been reported to target SET/TAF-I β ³², an
73 oncoprotein with histone chaperone activity involved in several biological processes^{36–}
74 ³⁸, including chromatin remodeling^{39,40} and DNA damage response (DDR)^{41,42}. In
75 particular, the ability of Cc to hinder SET/TAF-I β nucleosome assembly activity⁴³ and
76 also its role as protein phosphatase 2A (PP2A) inhibitor^{44,45} have been characterized.
77 Although SET/TAF-I β has not been reported to be involved in LLPS processes to date,
78 it is a well-known player in DNA damage foci—as the well-known phase-separating
79 factors fused-in-sarcoma (FUS) or p53-binding protein 1 (53BP1)^{3,17,46,47}—where
80 SET/TAF-I β retains DNA repair regulatory factors, such as heterochromatin protein 1
81 (HP1) family. HP1, which regulates DNA repair⁴¹ and heterochromatin organization,
82 exerts its function within LLPS compartments^{48,49}. Within this frame, questions arise
83 whether SET/TAF-I β undergoes phase separation in DNA foci.

84
85 SET/TAF-I β is a homo-dimer formed by coiled-coil interactions between the N-terminal
86 α -helical domains present in each monomer (Figure 1A, B). Each domain is followed by
87 a globular region, usually called the “earmuff” motif, and a C-end IDR consisting of
88 repeats of Asp and Glu³⁹. Both “earmuff” motifs and IDRs have been identified as the
89 carriers of histone chaperone activity^{39,50} and Cc-binding ability^{43,44}. NPM1 is a homo-
90 pentamer assembled by the N-terminal domains, which present a β -barrel architecture
91 (Figure 1A, C). This is followed by a histone-binding domain, which is an IDR
92 composed of alternating acidic and basic stretches, connected to a small globular C-
93 end DNA binding domain⁵¹. NPM1 has been described as a “scaffold” molecule⁵² of the
94 nucleolus, being essential for its structural integrity and one of the main responsible for
95 its assembly and function^{53,54}. In fact, the NPM1 pentameric state is important for its
96 nucleolar localization⁵⁵. Pentamerization, along with DNA binding domains, powers
97 NPM1 multivalency and allows it to undergo LLPS, mainly through its IDR enriched not
98 only in “D/E-tracts”, but also in “K-blocks”^{14,54,55}. NPM1 “D/E-tracts” and “K-blocks”,
99 together with adjacent Arg residues (Figure S1), allow the assembly of NPM1
100 coacervates by establishing homo-⁵⁶ and heterotypic interactions, either with other
101 NPM1 molecules or with other partners, such as ARF⁵⁷ or Cc³⁴.

102
103 Our former research work showed that Cc binds both SET/TAF-I β and NPM1 proteins
104 mainly through the surface amino acids surrounding the heme group^{34,43,44}. This
105 surface is characterized by a prominent positive electrostatic potential, as it hosts 18
106 lysine amino acids out of the total 104 Cc residues. Such lysine residues play a pivotal
107 role in the interactions involving Cc, most of which are based on electrostatics^{32,58,59}.
108 Most of these lysines are exposed to the solvent and grouped into clusters. Two of
109 these K-blocks deserve a special focus: i) the cluster composed of Lys5, Lys7 and Lys8
110 at the N-end of α_1 -helix; ii) the cluster comprising Lys86, Lys87 and Lys88 at the C-
111 terminal α_4 -helix, (Figure 2A). For simplicity, we will refer to them as the N-terminal and
112 C-terminal K-blocks, respectively. Both K-blocks have been shown to participate in the
113 binding interface with both SET/TAF-I β and NPM1^{34,43}, even though they show different
114 chemical-shift perturbations in each complex (Figure 2B, C). It is noteworthy that the N-

115 terminal K-block of Cc exhibits a similar topology and sidechain orientation as the C-
116 terminal domain of HDM2 (Figure S2) that, upon being recognized by NPM1, prevents
117 the binding of HDM2 to p53, thus stabilizing the tumor suppressor protein⁶⁰.
118 Furthermore, the segment comprising residues 86-101—which contains the above-
119 mentioned C-terminal K-block—has been reported to be the minimal Cc unit capable of
120 inducing caspase activation⁶¹ and sufficient to define bioactive cell penetrating peptides
121 with which the hemeprotein could be directed towards the nucleus⁶¹.

122

123 In this work, we first report the ability of the oncoprotein SET/TAF-I β to phase separate
124 together with Cc. We use this model system, along with the previously reported
125 NPM1:Cc condensates, to delve deep into the molecular mechanisms by which the
126 aforementioned K-blocks in Cc mediate heterotypic phase separation transitions by
127 modulating i) intrinsic hemeprotein structural and dynamic properties, and ii)
128 recognition modes towards nuclear partners.

129

130 Results

131 SET/TAF-I β forms electrostatic condensates with cytochrome c by liquid-liquid 132 phase co-separation

133 The recruitment of DDR factors, such as SET/TAF-I β ⁴¹, to DNA foci occurs through
134 LLPS mechanisms⁶². Given the ability of mitochondrial, respiratory Cc to reach the cell
135 nucleus in response to DNA lesions and to interfere with SET/TAF-I β functioning⁴³, we
136 hypothesize that both Cc and SET/TAF-I β proteins are capable of assembling liquid-
137 like condensates.

138 A titration of SET/TAF-I β with Cc resulted in the formation of phase-separated liquid
139 droplets that hosted both proteins (Figure 3A). This process was clearly observed when
140 the molar SET/TAF-I β :Cc ratio was 1:8. Previously, we reported that Cc recognizes two
141 binding sites in dimeric SET/TAF-I β ⁴³, sampling the “earmuff” interfaces and the C-end
142 tails of the chaperone. Then, SET/TAF-I β :Cc phase co-separation requires partial
143 charge compensation of the anionic disordered tail of SET/TAF-I β , although still leaving
144 unsatisfied valences (i.e., charged amino acids or patches that are available for
145 interaction) to maintain droplet fluidity⁶³. The inability of SET/TAF-I β or Cc to phase
146 separate alone—even in the presence of crowding agents, such as Ficoll⁶⁴ (Figure
147 S3)—confirms that the interaction between the two proteins triggers condensate
148 assembly.

149 SET/TAF-I β is a histone chaperone which exhibits a strong negative electrostatic
150 potential surface that hinders protein PS via homotypic interactions (Figures 3B and
151 S1). However, the C-end Asp/Glu-rich IDRs of SET/TAF-I β , which bind to Cc^{43,44} and
152 show multivalent nature, may contribute to heterotypic contacts with Cc and, therefore,
153 liquid condensate formation. Actually, titrating a SET/TAF-I β construct lacking its C-end
154 IDRs (SET/TAF-I β Δ C) with Cc resulted in liquid droplets only at very high SET/TAF-
155 I β Δ C:Cc molar ratios (1:24, Figures 3C and S4). This finding reveals the paramount
156 importance of the disordered, negatively charged C-tails of SET/TAF-I β in its Cc-
157 mediated phase separation (Figures 3C and S4).

158 SET/TAF-I β :Cc enriched droplets are sensitive to NaCl (100 mM), thus confirming their
159 electrostatic nature (Figure S4C). Complete abolition of liquid-like droplets occurred in
160 the presence of SET/TAF-I β Δ C and Cc at 100 mM NaCl (Figure S4C). This is
161 consistent with our former results on the breaking off of the SET/TAF-I β Δ C:Cc complex
162 with high ionic strength, but not the SET/TAF-I β :Cc ensemble^{43,44}. This finding confirms
163 that the disordered, multivalent and anionic C-end tails of SET/TAF-I β act as
164 scaffolding unit of the electrostatic droplet network together with Cc.

165

166 K-blocks of cytochrome c prompt phase co-separation with histone chaperones

167 To explore whether Lys-based stickers of Cc are responsible for PS together with its
168 nuclear targets SET/TAF-I β or NPM1, the two N-end or C-end K-blocks were mutated
169 by Ala residues (Figures S5 and S6). Both histone chaperones were titrated with wild-
170 type (WT), K5A/K7A/K8A or K86A/K87A/K88A Cc variants, to monitor droplet growth
171 and quantify them under different ionic strength conditions (Figure 4).

172 The removal of Cc K-blocks substantially decreased the number of condensates in the
173 presence of SET/TAF-I β or NPM1, being almost absent in those assays that include the
174 K5A/K7A/K8A Cc mutant (Figure 4). In the presence of K86A/K87A/K88A Cc mutant, a
175 slight increase of phase separation was observed for chaperone:Cc molar ratios up to
176 1:16 and 1:24 with SET/TAF-I β and 1:10 with NPM1. However, these biomolecular
177 condensates show irregular shapes that more closely resemble solid-like aggregates
178 than liquid phase-separated bodies.

179 Condensates harboring triple Lys-to-Ala Cc mutants, along with SET/TAF-I β , were still
180 sensitive to ionic strength despite having neutralized three positive charges each, as
181 their size and abundance decreased in a NaCl-concentration dependent manner (from
182 50 to 100 mM NaCl, Figure 4B). This suggests that i) both N-end and C-end K-blocks
183 are necessary for droplet assembly in agreement with reported nuclear magnetic
184 resonance (NMR) data^{34,43} (Figure 2B, C); and ii) they are not sufficient and other
185 lysine residues scattered on Cc surface may be involved in binding and phase
186 separation with SET/TAF-I β . For liquid droplets involving NPM1, a fixed ionic strength
187 (100 mM NaCl) was kept in all experiments to ensure, on one hand, the stability and
188 consequent functionality of the NPM1 pentamer⁵⁵ and, on the other hand, experimental
189 conditions to guarantee that NPM1 phase separates⁵⁶ (Figure 4D).

190 Consistently, triple Lys-to-Ala Cc mutants have a significant impact in complex
191 formation with SET/TAF-I β and NPM1, as inferred from isothermal titration calorimetry
192 (ITC) (Table 1, Figure S7). In particular, the binding affinity of complexes between
193 SET/TAF-I β and K5A/K7A/K8A or K86A/K87A/K88A Cc mutants decreased in an order
194 of magnitude with respect to those with WT Cc, followed by a drastic reduction in
195 cooperativity between the two binding sites for Cc on SET/TAF-I β surface. Such
196 synergy was completely abolished in ensembles involving the triple C-end Lys-to-Ala
197 Cc mutant, where the two-binding events were independent and enthalpically-driven
198 (Table 1). The thermodynamic profile of the interaction between K5A/K7A/K8A Cc and
199 SET/TAF-I β is entropically-driven, as occurs for WT Cc. Such thermodynamics
200 behavior is characteristic of electrostatically-guided adducts, due to the entropy
201 increase caused by the exclusion of water molecules surrounding charged, interacting
202 protein interfaces (see Supplementary Note S1). On the contrary, the global
203 thermodynamic endothermic-to-exothermic shift observed for the interaction involving
204 K86A/K87A/K88A Cc is consistent with a significant reduction of the aforementioned
205 desolvation—mainly due to the displacement of water molecules away from molecular
206 interface—, coupled to attenuated electrostatics. This is in accordance with the change
207 of electrostatic surface potential (ESP) of Cc induced by the K86A/K87A/K88A
208 mutation, which is more prominent than that of K5A/K7A/K8A Cc (Figure S8).
209 Moreover, the triple C-end Lys-to-Ala substitution may promote additional hydrophobic
210 interactions between Cc molecules, since the resulting K86A/K87A/K88A stretch would
211 be surrounded by other hydrophobic residues already present in WT Cc.

212 supported by the modifications in the ESPs of the different Cc species. If there are
213 other possible and more specific explanations—e.g. the predominance of weak
214 intermolecular forces, which take place with heat release, or the hydrophobic self-
215 association of mutant Cc molecules that we suggest—we can only speculate about
216 them.

217

218 Binding effects of triple Lys-to-Ala Cc mutants complexed with NPM1 were more
219 pronounced. While the K_D increased two orders of magnitude (from 6.5 to 300 μM) in
220 the complex with the K86A/K87A/K88A Cc mutant, no interaction was detected
221 between K5A/K7A/K8A Cc and NPM1 (Table 2, Figure S7).

222 Altogether, both N-end and C-end K-blocks are hallmarks of multivalency in Cc that
223 regulate its electrostatic coacervation in complex with SET/TAF-I β or NPM1.

224

225 **Molecular grammar of cytochrome c-containing condensates: the role of K-** 226 **blocks versus and R-blocks**

227 Despite the general, classical debate that lysine and arginine residues operate similarly
228 within proteins—due to their status as basic amino acids—many works have evidenced
229 that their divergent chemical characteristics make them different in terms of binding
230 and multivalency^{65,66}. As a consequence, they specifically drive different location and
231 functional propensities to the proteins by modifying their PS ability^{19,67}. To reveal
232 molecular mechanisms that lead Cc K-blocks to phase separate with SET/TAF-I β or
233 NPM1, triple Lys-to-Arg Cc mutants were designed (Figures S5 and S6).

234 Replacing Lys5, Lys7 and Lys8 of Cc by Arg residues resulted in an increase of
235 quantity and size of condensates—with respect to WT Cc—with either SET/TAF-I β or
236 NPM1 (Figure 5). Droplets enriched with SET/TAF-I β and K5R/K7R/K8R Cc remain
237 dependent on ionic strength (Figure 5B). Mutations of Lys86, Lys87 and Lys88 from Cc
238 by Arg almost abolished the condensation process, especially in the presence of
239 NPM1. Indeed, the occupied areas by droplets decreased ca. 10-fold at all molar ratios
240 (Figure 5).

241 Despite drastic consequences that triple Lys-to-Arg Cc mutants performed in
242 conducting PS with SET/TAF-I β or NPM1, slight differences in binding affinities were
243 determined between Arg-mutants or WT Cc with both chaperones. Their
244 thermodynamic profiles revealed, however, remarkable disparities in recognition modes
245 that could be underlying prominent changes in PS transitions, especially those
246 harboring SET/TAF-I β . ITC measurements showed that the SET/TAF-I β -binding
247 process of both Arg-Cc variants is enthalpically-driven ($\Delta H < 0$; $-T\Delta S > 0$), contrary to
248 what is found in that for WT Cc (Table 1, Figure S7), and typically in complexes
249 involving IDRs, electrostatic-based ensembles and then coacervation-mediated LLPS
250 events^{68–71}. Such enthalpically-driven thermodynamic profile has been ascribed to the
251 formation of weak interactions—such as H-bonds or van der Waals forces⁶⁸—involved
252 in intermolecular recognition (see Supplementary Note 1). The deconvolution of the
253 thermodynamic parameters of the SET/TAF-I β complexes with different Cc variants
254 rendered separately the values for the first interaction event and that affected by
255 cooperativity (Table S1). Whereas the first molecular-recognition event followed the
256 abovementioned thermodynamic behavior (governed by enthalpy; $\Delta H < 0$ and $-T\Delta S >$
257 0), the binding step governed by cooperativity became entropically driven ($\Delta H >$
258 0 ; $-T\Delta S < 0$).

259 To explain the inversion of the thermodynamic profile for the first binding event upon
260 replacement of Lys blocks by Arg, we further analyzed the intramolecular H-bonds
261 during molecular dynamics (MD) computed on Arg-variants. Indeed, Arg sidechains
262 established additional intramolecular H-bonds in the two K5R/K7R/K8R and
263 K86R/K87R/K88R Cc mutants (Figure S9A), although the total number of H-bonds
264 involving all potential donor/acceptor atoms of Cc remains constant when mutants are
265 compared with WT Cc (Figure S9B). Such an apparent compensation of the new H-
266 bonds rising in Cc Arg-mutants with respect to the WT lead to maintain the overall
267 folding of the hemeprotein. In particular, Arg5 is able to form largely represented H-
268 bonds with sidechains of Glu89 and Asp93, which are located at the Cc helix 4 (Figure
269 S9C). These weak H-bond contacts probably limit the mobility of helix 4 with respect to
270 helix 1 and, therefore, hinder the plasticity and dynamics of such motifs to recognize
271 SET/TAF-I β . Similarly, Arg7 and Arg87 establish H-bonds with sidechains of acidic
272 residues respectively placed at a distance of one helix turn, contributing to helix
273 stability (Figure S9C). Detailed data of H-bonds analyses on the different Cc variants
274 are given in Table S2. To make these sidechains available to chaperones, the
275 disruption of the abovementioned intramolecular contacts is first required. Thus, the
276 heat release observed for the first binding event ($\Delta H < 0$; Table S1) would respond to
277 the formation of energetically favorable interactions—either H-bonds or cation- π —
278 established by non-H-bonding Arg residues in Cc with acceptor residues of SET/TAF-
279 I β . This may explain the global endothermic-to-exothermic transition profile ($\Delta H <$
280 0 ; $-T\Delta S > 0$) showed by Cc Arg-mutants-dependent complexes. This phenomenon is
281 more pronounced for ensembles with K5R/K7R/K8R Cc, in agreement with the large
282 number and frequency of H-bonds formed by Arg sidechains and also the substantial
283 NMR chemical-shift perturbations (CSPs) experienced by residues 5 and 7, *vis-à-vis*
284 residue 87, in complex with SET/TAF-I β (Figure 2B, C).

285 Interestingly, the cooperativity makes the second binding event entropically driven (ΔH
286 > 0 and $-T\Delta S < 0$; Table S1), revealing multivalent recognition between positively-
287 charged R-blocks from Cc and anionic unstructured C-tails of SET/TAF-I β that lead to
288 the paradoxical disorder-to-order transition in droplets^{72,73}. The release of water
289 molecules from binding interfaces during PS may also contribute to a favorable
290 entropy⁷¹ (see Supplementary note S1). The molecular reorganization of SET/TAF-I β
291 was further confirmed by site-directed spin labeling electron paramagnetic resonance
292 (SDSL-EPR). Four single-Cys mutants on residues distributed along the SET/TAF-I β
293 IDRs—namely D226C, E243C, D260C and D277C—were designed and used for spin
294 labeling by MTSL. Continuous wave (CW) X-band EPR spectra of each spin-labeled
295 variant of SET/TAF-I β were recorded at room temperature, for the protein both alone
296 (80 μ M) and in complex with Cc (1:2 molar excess). EPR spectra of SET/TAF-I β alone
297 showed narrow lines indicative of high flexibility, due to the intrinsically disordered
298 nature of the domain. This flexibility was restricted for the D226C^{MTSL} species when
299 compared to the three other positions, showing some structural constraints consistent
300 with its location near the globular earmuff domains (Figure S10). When Cc was added,
301 the spectrum broadened for position 226, reflecting a decrease in label mobility. A
302 slight broadening was also observed for positions 243 and 260, indicating a local loss
303 of mobility for those residues placed at the central positions of the IDR. This indicates
304 that the dynamics of the middle IDR of SET/TAF-I β is restricted upon Cc binding
305 (Figure S10), in agreement with IDRs dynamics into condensates⁷⁴. Within this frame,
306 thermodynamic profiles inferred from the interaction of Arg-Cc variants on two

307 independent binding sites on NPM1 surface are also entropically-driven (Table 2,
308 Figure S7).

309 Changes in the ESPs of Cc upon Lys-by-Arg mutations (Figure S8) can modulate the
310 binding mode and phase separation properties of the hemeprotein with SET/TAF-I β
311 and NPM1. In addition, both Arg-mutants exhibited an increased global dynamic in
312 which the stretch comprising residues 20-65 was particularly mobile (Figure S11),
313 although the overall secondary structures remained unaltered, as inferred from far-UV
314 circular dichroism (CD) spectra (Figure S12) and MD trajectories (Figure S13). For
315 K86R/K87R/K88R Cc variant, its heme environment was slightly perturbed, as
316 demonstrated by NMR chemical-shifts of the Met80- ϵ CH₃ resonance (ca. -3.36 ppm
317 due to its chemical environment^{43,75}), corresponding to an axial ligand of ferrous heme
318 iron (Figure S14). However, the Cotton effect at the Soret-band absorption
319 wavelength⁷⁶—monitored by Vis-CD spectroscopy—suggested that the heme
320 coordination of oxidized Cc variants did not change (Figure S15A). Substantial
321 changes in the midpoint redox potential values of the Cc variants were also not
322 expected as they were completely oxidized or reduced upon addition of sodium
323 ferricyanide or ascorbate, respectively, as observed for most of c-type cytochromes^{77,78}
324 (Figure S15B). These subtle changes in the heme moiety upon replacement of the C-
325 terminal K-block by Arg, probably due to long-range dynamics effects, alter the heme-
326 surrounding binding interfaces—important for SET/TAF-I β or NPM1 binding^{34,43}—and
327 explain the decrease in PS involving this triple Cc mutant.

328 Despite Arg and Lys residues are both positively charged at physiological pH⁷⁹, the
329 guanidium group planarity contributes to delocalize the electron cloud and to form H-
330 bonds with perfect colinear angles^{66,80}. In MD calculations, the guanidium moiety shows
331 more propensity than amine groups to form H-bonds with negatively charged residues
332 at helices 1 and 4 in Cc. The arginines, along with their tendency of forming H-bonds,
333 neutralize part of the positive potential on the hemeprotein surface, in particular the
334 area surrounding positions 86-87-88 (Figure S9). In turn, this slightly weakens the
335 binding of K86R/K87R/K88R Cc to SET/TAF-I β and NPM1 (Tables 1 and 2). Indeed,
336 previous studies revealed that Lys87 and Lys88 of Cc underwent large CSPs upon
337 NPM1 binding^{34,43,44} (Figure 2B, C).

338 In addition, condensates harboring K5R/K7R/K8R Cc may contain unsatisfied
339 valences, as Arg5 and Arg7 are primarily involved in intramolecular H-bonding that
340 impairs binding to negatively charged residues from chaperones (Figure 2B, C) and
341 their valence satisfaction. This could explain that such condensates show more
342 tendency to wet the hydrophilic surface, without the need of building a complex network
343 composed by homo—neither Cc nor chaperones phase separate alone—and
344 heterotypic contacts, as previously proposed by Cremades and coworkers⁶³.

345 In other words, a K-block-based molecular grammar governs the driving forces for
346 binding and phase separation of Cc with its nuclear targets SET/TAF-I β and NPM1.

347

348 **Selective cytochrome c-mobility inside electrostatic coacervates harboring**
349 **SET/TAF-I β or NPM1**

350 To further explore the PS experienced by SET/TAF-I β and NPM1 with Cc or its Arg-
351 mutants, the dynamics of the proteins inside condensates have been characterized in
352 order to determine any potential correlation between such dynamics and the binding
353 characteristics of these protein complexes. Mobility of protein components inside
354 condensates was followed by fluorescence recovery after photobleaching (FRAP)
355 assays on droplets with Oregon Green 488-labeled SET/TAF-I β or NPM1 and Texas
356 Red-labeled Cc variants—all of them 10% labeled—in a 1:16 (SET/TAF-I β :Cc) or 1:10
357 (NPM1:Cc) molar ratios.

358 Droplets containing SET/TAF-I β showed low fluorescence recovery of the WT,
359 K5R/K7R/K8R and K86R/K87R/K88R Cc variants, with average mobile Cc fractions
360 between 21-23% (Figure 6A, Table S3). These FRAP profiles and time-course curves
361 are consistent with mature phase separation systems rather than highly fluid liquid
362 droplets^{81,82}, whose viscoelastic properties seem to agree with gelation or percolation
363 processes^{83,84}. Percolation events would be induced by a compact electrostatic network
364 built between SET/TAF-I β scaffolds and Cc variants, and intimately imbricated by the
365 addition of new intermolecular, multivalent contacts along with the entropically-driven
366 conformational rearrangement of SET/TAF-I β IDRs, as suggested by thermodynamics
367 and EPR assays^{74,85}. It is worth noting that K86R/K87R/K88R Cc exhibited a faster
368 recovery kinetics (average half-recovery time ($t_{1/2}$), 21.3 s), than WT and K5R/K7R/K8R
369 Cc ($t_{1/2}$, 47.8 and 42.4 s, respectively) (Table S3), likely due to larger K_D/ρ values
370 (Table S1), which in turn relates to fewer and smaller condensates (Figure 5A).

371 NPM1-harboring condensates clearly showed liquid-like behavior, with fluorescence
372 recovery rates ranging from 32% to 47% for different Cc variants^{82,86} (Figure 6B, Table
373 S4). The apparent enhanced mobility of K5R/K7R/K8R Cc variant could be explained
374 by the subordinate role played by the N-terminal Lys cluster of Cc—in comparison with
375 the C-end Lys stretch—in liquid-liquid phase separation with NPM1 (Figure 5B). In this
376 case, the fluorescence-recovery rate for both Lys-to-Arg Cc mutants was significantly
377 faster than that of the WT. Then, like complexes involving SET/TAF-I β , there is an
378 inverse relationship between $t_{1/2}$ values of Cc variants from FRAP assays and the K_D
379 values of their adducts with NPM1 (Table 2).

380 When fluorescence recovery from labelled SET/TAF-I β or NPM1 was monitored by
381 FRAP assays performed within the same condensates that were previously analyzed
382 for Cc, the mobility that both chaperones exhibited was negligible (Figure S16, Tables
383 S3 and S4). The high Cc concentration to induce coacervate assembly contributes to
384 saturate the pool of chaperone molecules, limiting their mobility inside droplets and
385 their exchange with the diluted phase. The slightly higher mobility observed for both
386 chaperones when phase-separated with WT Cc (Tables S3 and S4) might be explained
387 by a higher contribution of complex coacervation to their PS compared to that with Cc
388 Arg-mutants.

389

390 Discussion

391 In the last years, LLPS has emerged as a fundamental biophysical mechanism
392 underlying a wide variety of biological processes that need to be spatial-temporally
393 delimited from the general subcellular bulk. In particular, a wide variety of nuclear

394 proteins and complexes and their functionalities have been reported to be relevant
395 when delineated within condensates, either as organelle-entities or transient bodies,
396 such as nucleoli, nuclear speckles and paraspeckles, Cajal bodies, histone-locus
397 bodies, chromatin domains or condensates mediating transcription, DNA replication or
398 repair^{17,87}. Among them, the processing of chromatin both under homeostatic—e.g., for
399 heterochromatin assembly or transcription—or stress conditions—DNA damage
400 signaling and repair—requires the compartmentalization or exclusion by LLPS of a
401 wide multitude of effectors on DNA segments. Specifically, DNA damage responses
402 utilize a tightly orchestrated network of phase-separating proteins, nucleic acids and
403 the DNA damage-induced polymer poly(ADP-ribose) (PAR) to control genome integrity
404 in a highly specific manner¹⁷. PARs are formed locally at DNA-damage sites and recruit
405 a plethora of PAR-binding proteins—most of them are intrinsically disordered and
406 establish multivalent electrostatic interactions—to cluster the damaged DNA⁸⁸ and the
407 subsequent foci and repair effectors^{62,89}. Within this framework, the oncoprotein
408 SET/TAF-I β stands out as an IDR-containing chromatin remodeller³⁹ capable of
409 counteracting DNA repair in DNA foci⁴¹.

410 Here we report for the first time the ability of SET/TAF-I β to undergo PS upon binding
411 to Cc, which translocates to the nucleus soon after DNA damage and counteracts the
412 function of the histone chaperone in several manners^{43,44}. In this context, we find that
413 the acidic disordered C-tails of SET/TAF-I β —which are also essential for the
414 recognition of histones—play a capital role in PS by powering multivalency of
415 SET/TAF-I β . Then, the ability of Cc to form LLPS with SET/TAF-I β offers a potential
416 mechanism for Cc to be incorporated into DNA damage repair foci and interfere with
417 the SET/TAF-I β function. Similarly, the involvement of LLPS processes in nucleosome
418 assembly involving SET/TAF-I β and even Cc, cannot be ruled out at all.

419 Within this framework, we have investigated the molecular mechanisms used by Cc to
420 phase-separate with SET/TAF-I β and with its previously described PS-partner NPM1.
421 Building on previous evidence, we find that Lys residues scattered in clusters on Cc
422 surface mainly mediate binding and PS with both partners, being the holders of its
423 multivalency. In particular, two triple-Lys patches, placed at both its N-end and C-end
424 helices, act as essential PS stickers in uneven manners by virtue of their chemical
425 nature, orientation and structural dynamics. Observing the effect derived from the
426 replacement of K-blocks allowed us to discriminate the different functions
427 accomplished by them as powerful stickers in Cc. While the N-end K-block is directly
428 involved in protein recognition contacts, the C-end one is responsible for the dynamical
429 rearrangement of SET/TAF-I β that allows the cooperative and multivalent recognition of
430 the heme protein and then, phase separation. It is plausible that such a dynamical
431 rearrangement would allow the transition from allovalent—as observed for other
432 charged intrinsically disordered proteins containing repetitive sequence features⁹⁰—to
433 multivalent recognition of Cc by the SET/TAF-I β IDRs. Binding cooperativity then leads
434 to the entropy gain, which is characteristic of electrostatic-based multivalent IDR-
435 involving complexes^{72,73} and to the water exclusion that occurs upon condensation⁷¹
436 (see Supplementary Note S1). A simpler thermodynamic landscape was described by
437 NPM1-mediated complexes together with Cc variants. Two independent binding sites
438 on NPM1 are recognized by Cc, with a significant entropy gain upon complex
439 formation. This is consistent with the multivalency of NPM1 and its ability to phase

440 separate by itself—as widely demonstrated by other works^{54,56}—without the need for
441 another partner to induce dynamical rearrangements in the binding and subsequent
442 condensation. To sum up, we suggest that the N-end and C-end K-blocks of Cc acts as
443 primary stickers from which the droplet network harboring histone chaperones is built.
444 In the case of SET/TAF-I β , the recognition of the C-end cluster drives the dynamical
445 rearrangement of the chaperone that allows its phase transition.

446 Interestingly, phase transitioning of SET/TAF-I β requires Cc binding just to compensate
447 the remarkable negative ESP of the chaperone. A similar behavior may be shown by
448 the acidic Leu-rich nuclear phosphoprotein 32 (ANP32) family members A and B, being
449 unable to phase separate under molecular crowding conditions (data unpublished).
450 Like SET/TAF-I β , ANP32A and ANP32B are also nuclear targets of Cc that lack
451 positive R/K-tracts and have acidic, D/E-rich IDRs whose repulsion would minimize
452 homotypic contacts. The shielding of IDRs negative charges by Cc, which induces
453 molecular reorganization⁹¹, might also underlie a possible phase transition experienced
454 by this type of chaperones.

455 Replacing the Lys residues of Cc by Arg provided more details about the specific roles
456 played by both K-blocks. Being also a positively charged residue at physiological pH
457 due to its high pK_a ⁷⁹, primary electrostatics does not make the difference between Lys
458 and Arg. However, both type of residues exhibits very different chemical properties that
459 make them truly distinct as drivers of PS^{65–67}. First, the planarity of the guanidinium
460 group causes the electron cloud of ionized Arg to be delocalized, conferring it “Y-
461 aromaticity” and a directional preference to form cation- π interactions with aromatic—
462 Tyr and Phe—residues, in contrast to Lys^{65,80}. In addition, their ability to form H-bonds
463 is also substantially different. Arg-guanidinium possesses more atoms capable of
464 forming H-bonds—as reflected by the emergence of local H-bonds when Arg is
465 present—and does so with almost perfectly colinear angles. In contrast, despite being
466 less sterically constrained, Lys is only able to form one H-bond with optimal orientation,
467 as the formation of more than one is accompanied by angle distortions. For these
468 reasons, Arg is expected to establish stronger interactions within condensates⁶⁷. Thus,
469 ITC analyses of complexes between Cc Arg-mutants and SET/TAF-I β exhibited
470 thermodynamics consistent with the breakage and replacement of intramolecular
471 interactions established by Arg residues—reflected by MD—by the onset of new
472 intermolecular ones. Moreover, Arg at the N-end of Cc led to the greater formation of
473 condensates with both SET/TAF-I β and NPM1. Given the role of this Lys patch in direct
474 interaction with both chaperones, such effect is explained by the greater ability of Arg
475 to establish more H-bonds and strong cation- π interactions with Tyr sidechains⁹².
476 Substitution of the C-end Lys cluster by Arg did not compromise the effect of
477 cooperativity in the SET/TAF-I β recognition, but strongly abolished condensate
478 formation with both SET/TAF-I β and NPM1. We found that substitution of this Lys patch
479 led to long-range changes in the dynamics of Cc that affected the heme surroundings.
480 The C-end K-block is included, along with other Lys that are closer to the heme cleft, in
481 the interacting surface which Cc uses to recognize both histone chaperones^{34,43}. It is
482 then likely that the C-terminal Lys patch acts not only as a sticker but also as a spacer,
483 by controlling the appropriate orientation of other putative stickers distributed across
484 the Cc surface.

485 On another level, we observed differences in the dynamics of the condensates formed
486 by Cc with SET/TAF-I β or NPM1. We observed that Cc exhibited lower turnover in
487 condensates formed by SET/TAF-I β than in those assembled by NPM1. The faster Cc
488 dynamics into NPM1-containing condensates is in agreement with that of molecules
489 incorporating to scaffold-stablished condensates in the cell, usually diffusing fast⁵¹. This
490 is consistent with the ability of NPM1 to phase separate with itself and scaffold the
491 nucleoli. Indeed, the exchange of NPM1-associated factors between nucleoli and
492 nucleoplasm, including Cc, is well documented^{34,51}. In contrast, SET/TAF-I β :Cc
493 condensates exhibit low dynamics. Such a reduced turnover of protein molecules is
494 probably due to the coupling of gelation or percolation processes⁹³. The maturation of
495 LLPS into solid- or gel-like condensates has been observed as a part of both normal
496 and pathological biological responses³⁰. Some of these rheological evolutions act
497 reversibly to regulate cellular responses by constraining or loosening protein dynamics
498 within such condensates^{94,95}. Indeed, an example is that of HP1 α , whose phase-
499 separating dynamics fluctuations directly modulates the dynamics of heterochromatin⁹⁶.
500 Altogether, it is tempting to propose that the role of SET/TAF-I β within DNA foci would
501 be precisely to decrease their dynamics by itself—since it consists on arrest proteins
502 the DNA breaks⁴¹—or by incorporation of Cc. In support of this hypothesis, Cc has
503 recently been shown to increase the residence time of SET/TAF-I β on nucleosomes,
504 thereby slowing-down its turnover in the context of histone eviction and deposition⁹⁷. In
505 this context, it has been previously proposed that the concentration of Cc reaching the
506 nucleus may be variable and dependent on the level of DNA damage⁹⁸. Since high
507 stoichiometric amounts of Cc are required for PS with SET/TAF-I β , it could be
508 suggested that, under exacerbated DNA damage, PS provides a molecular mechanism
509 involving retention of chaperones in nucleosomes and blockage of repair of DNA.

510 In summary, we report here the case of a small and globular protein with sequence-
511 encoded heterotypic PS properties. Such phase transition capability is primarily
512 determined by Lys clusters distributed on its surface, which confers multivalency. In
513 addition, Cc represents a paradigm of an evolutionarily selected mechanism to perform
514 PS, both by virtue of its thermodynamic way to recognize its phase-separating partners
515 and its control of the intrinsic dynamics of the molecule. Furthermore, Lys expands the
516 regulatory span through protein post-translational modification (PTM), since it is a
517 substrate for many more types of PTMs than Arg and has been found to be modified
518 more frequently along the proteome⁹⁹. In fact, in the particular case of Cc, different Lys
519 acetylation and methylation have been detected affecting mitochondrial electron
520 transfer in different pathological contexts^{100–102}. Lysine succinylation of Cc has also
521 been reported, although specific functional effects of this PTM have not been further
522 investigated¹⁰³. In the context of PS, PTMs are being increasingly documented as a
523 mechanism by which multivalency of proteins PS is modified^{17,104}. Thus, a possible
524 relevance of Lys-PTMs over its LLPS ability and derived functions cannot be excluded.

525

526 **Limitations of the study**

527 The main goal of this study is to unveil the molecular mechanisms underlying protein
528 phase transitions *in vitro* using a biophysical approach. In particular, the article
529 focusses on those processes that govern the condensation of Cc together with its

530 nuclear targets under stress conditions. Whereas Cc undergoes phase transition
531 toward the nucleolus by binding to NPM1 to modulate the cellular DNA damage
532 response, further studies will be necessary to explore the co-phase separation of Cc
533 and SET/TAF-I β *in cell* and its biological relevance.

Journal Pre-proof

Figure Legends

Figure 1. Structural architecture of SET/TAF-I β and NPM1. (A) Domain organizations and (B, C) ribbon representation of structural models for (B) SET/TAF-I β and (C) NPM1. For the SET/TAF-I β model, dimerization domain (residues 1-80) is represented in light blue, the earmuff domain (81-225) in dark blue, and the acidic disordered domain (226-277) in coral. The structural model was built using MODELLER¹⁰⁵ to trace the earmuff loops and C-terminal unstructured stretches, which were absent in the crystallographic structure (PDB entry 2E50³⁹). For the NPM1 model, oligomerization domains forming a pentamer unit are represented in green (residues 1-130, PDB entry 4N8M⁵⁵), highlighting one monomer in dark green. The disordered histone-binding domain (residues 131-225) has not been modeled. The C-terminal nucleic-acid binding domain (residues 226-294, PDB entry 2LLH¹⁰⁶) is in grey.

Figure 2. Cytochrome c lysine clusters involved in the interaction with SET/TAF-I β and NPM1. (A) Ribbon representation of Cc (PDB entry 2N9I¹⁰⁷). Cc Lys clusters mutated in this study are shown. The N-terminal cluster containing Lys5, Lys7 and Lys8 is shown in cyan. The C-terminal cluster with Lys86, Lys87 and Lys88 is highlighted in purple. The last Lys-stretch is part of the minimal unit of Cc defined as a cell-penetrating peptide (residues 86-92⁶¹). (B) ¹H chemical-shift perturbations (¹H $\Delta\delta$) of amide resonances of Lys residues of ¹⁵N-labelled Cc upon titrating with SET/TAF-I β (*left*) or NPM1 (*right*), inferred from ¹H-¹⁵N HSQC NMR spectra^{34,43}. Bars are colored according to ¹H $\Delta\delta$ (ppm) values: white for <0.020, yellow for \leq 0.040, orange for \leq 0.080, red for \leq 0.100. (C) Surface mapping of ¹H $\Delta\delta$ underwent by Lys amide residues located at the N-end and C-end clusters of Cc (PDB entry 2N9I¹⁰⁷) upon complex formation with SET/TAF-I β (*left*) or NPM1 (*right*). Lys are colored following the same code as in panel B.

Figure 3. SET/TAF-I β phase separates upon binding to cytochrome c. (A) Fluorescence confocal microscopy images of phase separation by 10 μ M SET/TAF-I β with 80 μ M Cc. SET/TAF-I β was labeled with Oregon Green 488 (green) and Cc, with Texas Red-succinimidyl ester (red). Scale bars are 10 μ m. (B) Electrostatic surface potential map of SET/TAF-I β , calculated at 15 mM ionic strength. (C) DIC microscopy images of droplets formed by 10 μ M either SET/TAF-I β or SET/TAF-I β Δ C with 80, 160 or 240 μ M Cc (chaperone:Cc molar ratios of 1:8, 1:16 and 1:24). Scale bars are 30 μ m.

Figure 4. Effects of Lys-to-Ala substitutions of cytochrome c on its ability to phase-separate with SET/TAF-I β and NPM1. (A) Fluorescence and DIC microscopy images of condensates driven by 10 μ M SET/TAF-I β with 160 μ M WT, K5A/K7A/K8A or K86A/K87A/K88A Cc variants (1:16 molar ratio). SET/TAF-I β was used as 90% unlabeled SET/TAF-I β and 10% SET/TAF-I β Q69C mutant labeled with Oregon Green 488 (green). Scale bars are 30 μ m. (B) Percentage of area in the microscopy field occupied by protein condensates as a function of both the chaperone:Cc molar ratio (10 μ M SET/TAF-I β) and NaCl concentration. WT, K5A/K7A/K8A and

K86A/K87A/K88A Cc variants are at the upper, middle and lower histograms, respectively. Error bars represent the standard deviation (SD) calculated from 10 images per each protein complex. **(C)** Fluorescence and DIC microscopy images of condensates driven by 10 μ M NPM1 with 50 μ M WT, K5A/K7A/K8A or K86A/K87A/K88A Cc variants (1:5 molar ratio). NPM1 was used as 10% labeled with Oregon Green 488 (green). Scale bars are 30 μ m. **(D)** Percentage of area in the microscopy field occupied by protein condensates as a function of chaperone:Cc molar ratio with 10 μ M NPM1 at 100 mM NaCl. Error bars represent the SD from 10 images per each protein complex.

Figure 5. Effects of Lys-to-Arg substitutions of cytochrome c on its ability to phase-separate with SET/TAF-I β and NPM1. **(A)** Fluorescence and DIC microscopy images of condensates driven by 10 μ M SET/TAF-I β with 160 μ M K5R/K7R/K8R or K86R/K87R/K88R Cc variants (1:16 molar ratio). SET/TAF-I β was used as 90% unlabeled SET/TAF-I β and 10% SET/TAF-I β Q69C mutant labeled with Oregon Green 488 (green). Scale bars are 30 μ m. **(B)** Percentage of area in the microscopy field occupied by protein condensates as a function of both the chaperone:Cc molar ratio (10 μ M SET/TAF-I β) and NaCl concentration. Error bars represent the standard deviation (SD) calculated from 10 images per each protein complex. **(C)** Fluorescence and DIC microscopy images of condensates driven by 10 μ M NPM1 with 50 μ M K5R/K7R/K8R or K86R/K87R/K88R Cc variants (1:5 molar ratio). NPM1 was used as 10% labeled with Oregon Green 488 (green). Scale bars are 30 μ m. **(D)** Percentage of area in the microscopy field occupied by protein condensates as a function of chaperone:Cc molar ratio with 10 μ M NPM1 at 100 mM NaCl. Error bars represent the SD from 10 images per each protein complex.

Figure 6. FRAP measurements on droplets assembled by cytochrome c variants with SET/TAF-I β or NPM1. **(A)** Fluorescence recovery of ROIs (cyan dashed squares) from droplets containing fluorescent labeled WT, K5R/K7R/K8R or K86R/K87R/K88R Cc variants in complex with SET/TAF-I β (*left panel*) or NPM1 (*right panel*). Confocal microscopy images are shown before bleaching (prebleach state) and 3, 10 and 75 s postbleaching. Scale bars are 1 μ m. **(B)** Kinetics of labeled Cc fluorescence emitted from the bleached regions of droplets containing SET/TAF-I β (*left panel*) or NPM1 (*right panel*), after background subtraction and normalization of intensities. Coral shadows represent the standard error of the mean (SEM) for 4 or 5 droplets per protein complex.

Tables

Table 1. Thermodynamic parameters of SET/TAF-I β in complex with cytochrome c variants. Calculated equilibrium intrinsic dissociation constants (K_D), Gibbs free energy (ΔG), association enthalpy (ΔH), entropic term ($-T\Delta S$), active protein fraction (n) and cooperativity factor (ρ) are displayed for SET/TAF-I β reactions with WT or Lys-mutated Cc variants. Relative errors are less than 20% for K_D and 10% for ΔH . These values are provided by the fit to a two cooperative-binding sites model for complexes involving WT, K5A/K7A/K8A, K5R/K7R/K8R and K86R/K87R/K88R Cc, or to a set of identical and independent binding sites model for the K86A/K87A/K88A Cc:SET/TAF-I β complex.

Protein complex	K_D (μ M)	ΔG (kcal/mol)	ΔH (kcal/mol)	$-T\Delta S$ (kcal/mol)	n	ρ
WT Cc:SET/TAF-I β	3.6	-7.43	1.30	-8.73	1.2	1.24
K5A/K7A/K8A Cc:SET/TAF-I β	45.5	-5.92	5.70	-11.62	0.9	0.52
K5R/K7R/K8R Cc:SET/TAF-I β	2.0	-7.77	-15.00	7.23	1.1	0.76
K86A/K87A/K88A Cc:SET/TAF-I β	40.0	-6.00	-6.10	0.10	2.3*	-
K86R/K87R/K88R Cc:SET/TAF-I β	5.9	-7.13	-7.70	0.57	1.1	0.80

* n stands for the binding stoichiometry in the K86A/K87A/K88A Cc:SET/TAF-I β complex, with independent binding sites.

- Not applicable

Table 2. Thermodynamic parameters of NPM1 in complex with cytochrome c variants. Calculated equilibrium dissociation constants (K_D), Gibbs free energy (ΔG), association enthalpy (ΔH), entropic term ($-T\Delta S$) and reaction stoichiometry (n) are displayed for NPM1 reactions with WT or its Lys-mutated Cc variants. Relative errors are less than 20% for K_D and 10% for ΔH . These values are provided by the fitting to a set of identical and independent binding sites model.

Protein complex	K_D (μ M)	ΔG (kcal/mol)	ΔH (kcal/mol)	$-T\Delta S$ (kcal/mol)	n
WT Cc:NPM1	6.5	-7.06	0.6	-7.66	1.9
K5A/K7A/K8A Cc:NPM1	No interaction				
K5R/K7R/K8R Cc:NPM1	14.0	-6.61	0.60	-7.21	2.0
K86A/K87A/K88A Cc:NPM1	300.0	-4.81	7.20	-12.01	2.0
K86R/K87R/K88R Cc:NPM1	15.0	-6.57	2.30	-8.87	1.8

STAR Methods

RESOURCE AVAILABILITY

Lead contact

Further information and requests for resources and reagents should be directed to and will be fulfilled by the lead contact, Prof. Irene Díaz-Moreno (idiazmoreno@us.es).

Materials availability

SET/TAF- β and cytochrome *c* clones, and all resources will be made available upon request.

Data and code availability

- All data will be shared by the lead contact upon request.
- This paper does not report original code.
- Any additional information required to reanalyze the data reported in this paper is available from the lead contact upon request.

METHOD DETAILS

DNA constructs

For recombinant expression of full-length SET/TAF- β , SET/TAF- β Δ C and NPM1, plasmids previously constructed were used^{32,34,39}. Genes encoding the abovementioned constructs were subcloned along with a N-terminal 6xHis tag, into a pET28a(+)-SET/TAF- β and NPM1—or a pET14b-SET/TAF- β Δ C—under the T7 promoter.

Cys single mutations were introduced by single mutations at different positions in SET/TAF- β to graft the MTSL nitroxide probe. Site-directed mutagenesis was performed by polymerase chain reaction (PCR), using the pET28a(+)-SET/TAF- β construct. The following primers were designed:

5'-CCAACCATTTTTTTGCAAGAGGTCAGAA-3' and
 5'-TTCTGACCTCTTGCAAAAAAATGGTTGG-3' for the Q69C mutation;
 5'-GTTCCCGATATGTGTGATGAAGAAGG-3' and
 5'-CCTTCTTCATCACACATATCGGGAAC-3' for D226C;
 5'-GATGAAGAGGAGTGCGGATTAGAAGAT-3' and
 5'-ATCTTCTAATCCGCACTCCTTTCATC-3' for E243C;
 5'-GAAGGTGAAGAATGTGAAGATGATGATG-3' and
 5'-CATCATCATCTTCACATTCTTCACCTTC-3' for D260C; and
 5'-GAAGGAGAAGATTGCTAACTCGAGCAC-3' and
 5'-GTGCTCGAGTTAGCAATCTTCTCCTTC-3' for D277C.

The DNA encoding for Cc was already cloned into the pBTR1 expression vector, along with the *CYC3* gene, encoding for yeast heme lyase for the proper heme group assembly and protein folding¹⁰⁸.

The Cc K5A/K7A/K8A mutant was obtained by three successive steps of site-directed mutagenesis, using PCR with the primers 5'-GACGTGGAAAAGGGCGCGAAGATCTTCATCATG-3' and 5'-CATGATGAAGATCTTCGCGCCCTTTCCACGTC-3' to mutate Lys7, secondly 5'-GCGCGGCGATCTTCATCATGAAATGCTCGCAGTGCCACA-3' and 5'-AGATCGCCGCGCCCTTTCCACGTCGCC-3' to mutate Lys8, and finally 5'-CGACGTGGAAGCGGGCGGGCGATCTTC-3' and 5'-GAAGATCGCCGCGCCCGCTTCCACGTCG-3' for Lys5 replacement.

For the construction of expression plasmids for K5R/K7R/K8R and K86A/K87A/K88A Cc mutants, gBlocks for each of the genes were acquired from Integrated DNA Technologies, Inc (IDT). Such DNAs were amplified by PCR with the primers 5'-CCATGGATGGGCGACGTGG-3' and 5'-GGATCCTCATTTCGTTTCGTCGCC-3', and subcloned into the pLW01 bacterial expression vector¹⁰⁹, using NcoI and BamHI restriction enzymes (*New England Biolabs*).

The gene encoding the Cc K86R/K87R/K88R mutant was amplified using the oligonucleotides 5'-GAAGGAGATATATCCATGGGCGACGTGGAAAAG-3' and 5'-CATCTTGGTACCTTATCATTTCGTTTCGTCGCCCTTT-3' and cloned into a linearized pBTR1 vector using the In-Fusion™ Snap Assembly EcoDry system (*Takara Bio*). pBTR1 was linearized by PCR with the primers 5'-TAAGGTACCAAGATGG-3' and 5'-GGATATATCTCCTTCTTAAAG-3'.

Protein expression and purification

SET/TAF-I β full-length and Δ C constructs, their respective Q69C mutants, D226C, E243C, D260C and D277C SET/TAF-I β , and NPM1 were expressed in the *E. coli* BL21(DE3) strain. Firstly, lysogeny-broth (LB) pre-cultures supplemented with kanamycin (50 μ g/mL)—for full-length SET/TAF-I β and NPM1—or ampicillin (100 μ g/mL)—for SET/TAF-I β Δ C constructs expression—were grown at 37 °C up to saturation. Afterwards, they were used to inoculate the final cultures, which were grown at 37 °C until an optical density measured at 600 nm (OD₆₀₀) of 0.6-0.8 was reached. 1 mM isopropyl- β -D-1-thiogalactopyranoside (IPTG) was then added to induce protein expression over night at 30 °C.

WT Cc and K5A/K7A/K8A mutant were expressed in the *E. coli* BL21(DE3) strain, as previously described¹¹⁰. Briefly, LB precultures supplemented with ampicillin (100 μ g/mL) were grown at 37 °C up to saturation. Then, 2.5 mL were used to inoculate 2.5 L cultures in 5 L Erlenmeyer flasks. For the expression of the K86R/K87R/K88R variant, single colonies were inoculated in 4 L LB cultures contained in 5 L Erlenmeyer flasks, so as to get semi-anaerobic growth conditions. These cultures were incubated over night at 30 °C under agitation. The expression of Cc K5R/K7R/K8R and K86A/K87A/K88A mutants was performed in C43(DE3) *E. coli* cells. Terrific-broth (TB) precultures supplemented with ampicillin (100 μ g/mL) and 1% glucose were grown at 37 °C up to saturation. Then, TB 1 L cultures contained in 2 L Erlenmeyer flasks were inoculated with 5 mL of preculture and grown at 37 °C until an OD₆₀₀ of 0.6-0.8. Expression was induced with 0.5 mM IPTG and cultures were incubated over night at 30 °C.

After expression, cells were harvested by centrifugation at 4,500 x g for 10 min (4 °C) and then, resuspended in lysis buffer, consisting on 20 mM Tris-HCl buffer (pH 8.0), 800 mM NaCl and 10 mM imidazole for SET/TAF-I β and NPM1 proteins or 10 mM tricine-NaOH (pH 8.5) for Cc constructs. Cell suspensions were treated during 15 min at room temperature with 0.2 mg/mL lysozyme and 0.02 mg/mL DNase I, in the presence of 0.01% phenylmethylsulfonyl fluoride (PMSF) and cOmplete™ Mini, EDTA-free, protease-inhibitor mixture (*Roche*). Then, cells were sonicated for 4 min (30"/45" cycles, 35% amplitude). Cellular debris was removed by centrifugation at 48,000 x g for 30 min (4 °C).

SET/TAF-I β and NPM1 proteins were purified from the protein extracts by affinity chromatography, using a HisPur™ Ni-NTA resin (*Thermo Scientific*) precharged column. For SET/TAF-I β Cys mutants, 5 mM dithiothreitol (DTT) was present during both bacterial lysis and protein purification. Cc purification was based on cation exchange chromatography, using a *Foresigth Nuvia S* 5 mL column (*BioRad*). The purity and homogeneity of protein preparations were tested by SDS-PAGE. SET/TAF-I β and NPM1 protein concentrations were measured by the Bradford method¹¹¹. Cc concentrations were determined by UV-Vis spectrophotometry, using an extinction coefficient at 550 nm of 28.92 mM⁻¹ cm⁻¹ for the reduced state of the heme protein. Proteins were concentrated using 3 or 10 kDa cut-off *Merck Millipore* concentrators and dialyzed against 10 mM sodium phosphate buffer (pH 7.4).

Circular dichroism spectroscopy

CD spectra of the WT and mutants Cc were recorded at 20 °C in the far UV region (190-250 nm) or in the visible (300-600 nm) at 0.2 nm/min, using a 1-mm thick quartz cuvette on a J-815 CD Spectropolarimeter (*Jasco*), equipped with a Peltier temperature control system. Measurements were taken for 10 μ M Cc in the far UV or 30 μ M Cc in the visible region. In all cases, samples were in 10 mM sodium phosphate (pH 7.4) buffer, containing a 10-fold molar excess of potassium hexacyanoferrate (III). Twenty scans were averaged for each sample.

Mass spectrometry

Mass spectrometry assays were performed at the Biomolecular mass, proteomics and metabolomics (BIO-MS) laboratory at the University Pablo de Olavide.

For in-solution protein samples, measurements were performed using a MALDI-TOF Ultraflextreme system (*Bruker*) configured on positive linear mode. For each spectrum, results of 3000 laser shots were averaged. A 1:10 mixture of α -cyano-hydroxycinnamic acid and 2,5-dihydroxybenzoic acid (20 mg/mL) was used as MALDI matrix. This matrix was in turn mixed with the sample, in a 1:2 (v/v) ratio and 0.5 μ L were deposited on a film of α -cyano-hydroxycinnamic acid and air-dried at RT.

To identify the corresponding mutations of each Cc variants, they were subjected to tryptic digestion. Acrylamide gel bands were detained with ammonium bicarbonate and acetonitrile. DTT and iodoacetamide were respectively used to break disulphide bonds

and carbamidomethylate cysteine residues. Samples were incubated overnight at 37 °C with bovine trypsin or at room temperature with chymotrypsin (K5R/K7R/K8R mutant), at ratio 1:10 (enzyme:substrate). After acetonitrile extraction and acidification, samples were desalted and concentrated with C18-filled tips.

Fingerprint MALDI measurements on Cc K86A/K87A/K88A and K86R/K87R/K88R mutants, positive reflectron mode was used. The results of 3000 laser shots were averaged for each spectrum. Measurements on Cc K5A/K7A/K8A and K5R/K7R/K8R mutants were performed with an Orbitrap Q-Exactive Plus mass spectrometer coupled to an Easy-nLC liquid nanochromatograph (Thermo Scientific). Tryptic digestion peptides were separated using a 50 cm C18 EASY-Spray column coupled with a C18 PepMap100 2 cm pre-column. A non-linear gradient was used between phase A (0.1% formic acid) and phase B (80% acetonitrile, 20% water, 0.1% formic acid) during 120 min in reverse phase mode. Then, top 10 MS/MS spectra were acquired in data-dependent acquisition (DDA) mode. Spray voltage was fixed at 2.9 kV and capillary temperature at 300°C. Maximum IT was set at 30 ms.

LC-MS data were analyzed using the SEQUESTTM HT search engine (Thermo Scientific). The following aminoacid modifications were considered in the analysis: static carbamidomethylation (Cys), dynamic oxidation (Met) and dynamic acetylation (N-termini). Data were searched against specific protein sequences for each mutant and results were filtered using a 0.01% protein false-discovery rate (FDR) threshold.

Protein spin labeling

SET/TAF-I β Cys mutant samples were dialyzed against 20 mM sodium phosphate (pH 7.4) and 50 mM NaCl, containing 1 mM of DTT. After the removal of DTT by gel filtration with a desalting PD-10 column (*GE Healthcare*), the nitroxide spin label MTSL ([1-oxyl-2,2,5,5-tetramethyl- δ 3-pyrroline-3-methyl] methanethiosulfonate; *Toronto Research Chemicals Inc.*, Toronto, Canada) was added to the sample at 7 to 10-fold molar excess from concentrated stock solutions in acetonitrile. The labeling reaction was carried out at 4 °C, in the dark, under gentle stirring and continuous flow of Ar during 1 h. Excess of unbound label was removed using a desalting column (PD-10) in 10 mM sodium phosphate, pH 6.3. The fractions containing the labeled variants were pooled and concentrated using 30 kDa cut-off *Merck Millipore* concentrators.

Electron paramagnetic resonance

CW-EPR experiments were performed on spin-labeled SET/TAF-I β single-Cys mutants, in both the absence and the presence of reduced Cc in a 1:2 SET/TAF-I β :Cc molar ratio. EPR spectra were recorded at 23°C on an ELEXSYS E500 *Bruker* spectrometer, equipped with a Super High Q Sensitivity resonator, operating at X-band (9.9 GHz). The microwave power was 10 mW, the magnetic field modulation amplitude 0.1 mT and the frequency modulation 100 kHz. Spin concentration was obtained by measuring the double integral of EPR signals, compared to a reference sample. Spin-labeling yields ranging from 80 to 100% were obtained for all variants.

Nuclear magnetic resonance

1D ^1H NMR spectra of the reduced Cc variants were acquired on a *Bruker* Avance III 500 MHz, equipped with a 5 mm TCI cryoprobe, at 25 °C. All samples contained 50 μM protein and 250 μM sodium ascorbate to ensure Cc was in a fully reduced state. Experiments were performed in 10 mM sodium phosphate buffer pH 7.4, containing 5% D₂O to adjust the lock signal. Water signal was suppressed by excitation sculpting method¹¹². Spectra acquisition and processing were made using TopSpin NMR software (*Bruker*).

Molecular dynamics computations

MD computations on Cc variants were performed with the OpenMM software¹¹³ in a CUDA platform. The initial structure of WT Cc was taken from the NMR model of human reduced Cc (PDB entry 2N9I¹⁰⁸). The models of simulated mutants were built based on the WT protein structure. All the topology and coordinate files were generated by using the LEAP module of the AMBER 16 package¹¹⁴ and the ff19SB force-field libraries¹¹⁵. Force-field parameters for the heme group¹¹⁶ were used to generate topology and coordinates.

Simulations were performed under periodic boundary conditions, using an orthorhombic cell geometry and particle mesh Ewald (PME) electrostatics with an Ewald summation cut off of 1 nm. The system was neutralized with sodium counterions according with the total charge of the protein and solvated using an optimal 3-charge, 4-point rigid water model (OPC) molecules¹¹⁷. For each system, evolution times of 1 μs were simulated at 298 K and 1 atm, with 2,500 previous energy minimization steps of 2 fs using a Langevin integrator¹¹⁸ with a friction coefficient of 1 ps^{-1} .

The PTRAJ module of AMBER¹¹⁹ was used for trajectory analysis. Molecular graphics were made with the UCSF Chimera 1.15 software¹²⁰.

Electrostatic surface potentials computations

The ESPs of SET/TAF-I β and the different Cc variants were calculated using the Adaptive Poisson-Boltzmann Solver (APBS, version 3.4.1)¹²¹ at 15 mM ionic strength. To do that, a structural model of SET/TAF-I β was built using MODELLER¹⁰⁵ to construct the absent stretches in the crystallographic structure (PDB entry 2E50³⁹). For Cc, structures resulting from 1- μs MD simulations of the WT protein and each mutant were used. Structures were prepared for APBS calculations by using the PDB2PQR (version 3.6.1) tool¹²². Surface mappings were made using the UCSF Chimera 1.15 software¹²⁰.

Isothermal titration calorimetry

ITC experiments were performed in a Nano ITC Low Volume (*TA Instruments*) at 25 °C. The experiments consisted of 20 injections of 300 μ M solutions of reduced WT or mutant Cc, 2.5 μ L each. The sample cell was initially filled with 20 μ M SET/TAF-I β or NPM1. All the experiments were performed in 10 mM sodium phosphate buffer pH 7.4, in the presence of 100 mM NaCl in titrations involving NPM1 so as to maintain its pentameric state⁵⁵. Injection interval was set to 180 s, allowing the return of the thermal power signal to the baseline before the next injection. During the titration, stirring was constantly maintained at 300 rpm. The reference cell was filled with ultra-pure water and all samples were degassed prior to the experiments. Injection heats normalized per mole of injectant *versus* molar ratio data were fitted to a set of independent and identical binding sites model or a two cooperative-binding sites model (see Supplementary Note S1).

Protein fluorescent labeling

Fluorescent labeling of SET/TAF-I β variants and NPM1 was performed by taking advantage of Cys residues to graft the fluorescent Oregon GreenTM 488 maleimide probe (*Molecular Probes*). SET/TAF-I β proteins labeling required the usage of their Q69C mutant, as the WT proteins lack Cys residues. NPM1 is labeled on its exposed Cys104. Proteins were dialyzed in 20 mM sodium phosphate (pH 7.4), 100 mM NaCl and 1 mM DTT. Then, DTT was removed by gel filtration using a desalting PD-10 column (*GE Healthcare*). Immediately, fluorescent probe was added at 10-fold molar excess from a concentrated stock solution in DMSO and the labeling reaction was performed for 2 h at RT in the dark, in 20 mM sodium phosphate buffer (pH 7.4) and 100 mM NaCl.

Cc WT and mutant variants were labeled with the Texas RedTM-X succinimidyl ester probe (*Molecular Probes*), which conjugates with non-protonated primary amine groups. Labeling reaction was carried out in 20 mM HEPES at pH 7.0, in order to maximize the protonation of Lys ϵ -amine groups and then restrict the labeling to the N-terminus of the protein. The reaction was incubated under agitation during 2 h at RT.

Excess of unbound labels was removed by extensive dialysis in 10 mM sodium phosphate (pH 7.4 buffer). Labeled proteins were concentrated in 10 kDa cut-off Amicon UltraTM centrifugal filters (*Merck*). Protein concentration and degree of labeling were determined by recording UV-visible spectra and following the manufacturer's indications.

Phase separation assays and imaging

Droplet formation was performed by mixing unlabeled SET/TAF-I β , SET/TAF-I β Δ C or NPM1 at a final concentration of 10 μ M with Cc variants at the indicated molar ratios, in 10 mM sodium phosphate (pH 7.4) buffer. When specified, a final concentration of 50 or 100 mM NaCl, or 15% Ficoll^R PM70 (*Cytiva*) was included. For fluorescence droplet analysis, fluorescently-labeled proteins were included in samples to represent 10% of the respective partner. The samples were equilibrated at RT for 5 min and then mounted in sealed chambers, composed of a glass slide and coverslip and kept

together by a layer of pierced 3M™ double-sided, 100- μ m thick tape. Once mounted, samples were equilibrated again during 10 min.

Samples were imaged at RT at a Leica DM6000B (*Leica Microsystems*) fluorescence microscope, using a 40x objective and an ORCA-ER camera (Hamamatsu). Differential interference contrast (DIC) and fluorescence filters FITCL5 filter (excitation band-pass, 480/40; emission band-pass, 527/30) and a Tx2 filter (excitation, 560/40 nm; emission, 645/75 nm) to visualize Oregon Green 488 and Texas Red, respectively were used when indicated. Images were processed and analyzed with the LAS X (*Leica Microsystems*) and the FIJI (ImageJ)¹²³ software packages.

Fluorescence recovery after photobleaching

Samples for FRAP measurements in liquid condensates were prepared as described in the previous section. Experiments were performed by a Leica TCS SP5 (*Leica Microsystems*) laser-scanning confocal microscope, using a 63x/1.4 oil immersion objective. Droplets suitable for FRAP measurements were preselected.

ROIs of 0.854 x 0.787 μ m covering a fraction of the selected condensate were bleached first with the 561-nm and then with the 488-nm laser lines—to avoid FRET-induced artifactual bleaching on the red channel—at 40% or 100% laser power, respectively. The bleaching protocol was as follows: three pre-bleaching images, five bleaching pulses at the indicated laser power and 100 post-bleaching images were taken every 774 ms. Images were collected using the Leica LAS-AF (*Leica Microsystems*) software, recording emitted fluorescence between 592-632 nm for the red channel and 497-552 nm for the green channel.

Mean fluorescence-intensity of ROIs inside bleached droplets and regions around them (as a control) were measured before and after bleaching. As well, mean fluorescence intensity of nonbleached droplets and the background fluorescence outside droplets were also recorded as controls. Fluorescence intensities were measured using the FIJI (ImageJ)¹²³ software package.

The normalized intensity was plotted over the time in the different FRAP determinations, analyzing 5 droplets for each protein complex. Normalized intensity over the time was fitted to a single exponential function ($y = y_0 + A*(1-e^{-kt})$), being “A” the plateau intensity and “k” a fitting constant. Recovery half times were calculated as $\ln(0.5)/-k$. Curve fittings and calculations were made using Origin 2018b (*OriginLab Corporation*).

QUANTIFICATION AND STATISTICAL ANALYSIS

Phase separation assays

For droplet quantification, 10 images were acquired and quantified per protein complex. The mean and standard deviation (SD) of droplet-occupied area were calculated. Images were processed and analyzed using the LAS X (*Leica Microsystems*) and the FIJI (ImageJ)¹²³ software packages.

Fluorescence recovery after photobleaching

For FRAP measurements, the normalized intensity was plotted over time, analyzing five droplets for each protein complex. Normalized intensity over time was fitted to a single exponential function ($y = y_0 + A \cdot (1 - e^{-kt})$), being “A” the plateau intensity and “k” a fitting constant. Recovery half times were calculated as $\ln(0.5)/-k$. Resulting parameters are presented as the mean \pm standard error of the mean (SEM). Images were processed and analyzed using the LAS X (*Leica Microsystems*) and the FIJI (ImageJ)¹²³ software packages. Data processing and fitting were performed using Origin 2018b (*OriginLab Corporation*).

Molecular dynamics: H-bonds calculations

Both the inter-residue (corresponding to Lys clusters) and the total intramolecular H-bonds information was extracted from 1- μ s MD trajectories, which were analysed using the PTRAJ module of AMBER¹¹⁹. Then mean and SD were calculated for both data sets and for each Cc variant.

Supplemental Information

Supplementary information contains Supplementary Note S1, figures S1–S16 and tables S1–S5.

Acknowledgements

This work was supported by the *Agencia Estatal de Investigación* (AEI), the Spanish Ministry of Science and Innovation (MCIN) and “ERDF A way of making Europe” (MCIN/AEI/10.13039/501100011033, grant number PID2021-126663NB-I00); the European Regional Development Fund (FEDER); the Andalusian Government (BIO-198); the University of Seville (VI PPIT) and the Ramón Areces Foundation. This work was also supported by Ministry of Education and Professional Training (FPU18/06577 for M.A.C.C.), Biointeractomics Platform (cicCartuja, Seville) and the NMR Services at CITIUS (University of Seville). The APC for open-access publication was funded by the University of Seville. For EPR studies, financial support from the IR INFRANALYTICS FR2054 for conducting the research is gratefully acknowledged. Authors also thank the COST MOBIEU (CA15126) for support in Short Term Scientific Missions. Molecular graphics and analyses performed with UCSF Chimera, developed by the Resource for Biocomputing, Visualization, and Informatics at the University of California, San Francisco, with support from NIH P41-GM103311. Authors thank to Dr. Ana Rodríguez-Hortal from the BIO-MS mass spectrometry at the University Pablo de Olavide (Seville) and Dr. Paloma Domínguez-Giménez at the CABIMER microscopy facility (Seville), as well as the microscopy and chromatography services from the Institute of Plant Biochemistry and Photosynthesis (Seville). We also thank Prof. Masami Horikoshi for the kind gift of the plasmid encoding SET/TAF-I β Δ C and Dr. Carlos A. Elena-Real for the construction of SET/TAF-I β Cys-mutants used in EPR experiments.

Author contributions

M.A.C.C.: Conceptualization, Data curation, Formal analysis, Investigation, Methodology, Software, Writing – original draft, Writing – review & editing, Visualization. **A.V.C.:** Formal analysis, Writing – review & editing. **M.M.:** Formal analysis. **V.B.:** Formal analysis, Writing – review & editing. **M.A.R.:** Conceptualization, Funding acquisition, Supervision, Writing – review & editing. **I.D.M.:** Conceptualization, Funding acquisition, Investigation, Project administration, Supervision, Writing – review & editing.

Declaration of interests

The authors declare no competing interests.

References

1. Banani, S. F., Lee, H. O., Hyman, A. A. and Rosen, M. K. (2017). Biomolecular condensates: Organizers of cellular biochemistry. *Nat. Rev. Mol. Cell Biol.* 18, 285. 10.1038/nrm.2017.7.
2. Shin, Y. and Brangwynne, C. P. (2017). Liquid phase condensation in cell physiology and disease. *Science*. 357, eaaf4382. 10.1126/science.aaf4382.
3. Laflamme, G. and Mekhail, K. (2020). Biomolecular condensates as arbiters of biochemical reactions inside the nucleus. *Commun. Biol.* 3, 1–8. 10.1038/s42003-020-01517-9.
4. O'Flynn, B. G. and Mittag, T. (2021). The role of liquid-liquid phase separation in regulating enzyme activity. *Curr. Opin. Cell Biol.* 69, 70–79. 10.1016/j.ceb.2020.12.012.
5. Mehta, S. and Zhang, J. (2022). Liquid–liquid phase separation drives cellular function and dysfunction in cancer. *Nat. Rev. Cancer* 22, 239–252. 10.1038/s41568-022-00444-7.
6. Brangwynne, C.P., Eckmann, C.R., Courson, D.S., Rybarska, A., Hoege, C., Gharakhani, J., Jülicher, F. and Hyman, A.A (2009). Germline P granules are liquid droplets that localize by controlled dissolution/condensation. *Science* 324, 1729–1732. 10.1126/science.1172046.
7. Mittag, T. and Parker, R. (2018). Multiple modes of protein-protein interactions promote RNP granule assembly. *J Mol. Biol.* 430, 4636–4649. 10.1016/j.jmb.2018.08.005.
8. Uversky, V. N. (2017). Intrinsically disordered proteins in overcrowded milieu: Membrane-less organelles, phase separation, and intrinsic disorder. *Curr. Opin. Struct. Biol.* 44, 18–30. 10.1016/j.sbi.2016.10.015.
9. Yasuhara, T. and Zou, L. (2021). Impacts of chromatin dynamics and compartmentalization on DNA repair. *DNA Repair (Amst)*. 105, 103162. 10.1016/j.dnarep.2021.103162.
10. Buchan, J. R., Yoon, J. H. and Parker, R. (2011). Stress-specific composition, assembly and kinetics of stress granules in *Saccharomyces cerevisiae*. *J. Cell Sci.* 124, 228–239. 10.1242/jcs.078444.
11. Fefilova, A. S., Fonin, A. V., Vishnyakov, I. E., Kuznetsova, I. M. and Turoverov, K. K. (2022). Stress-induced membraneless organelles in eukaryotes and prokaryotes: bird's-eye view. *Int. J. Mol. Sci.* 23, 5010. 10.3390/ijms23095010.
12. Mohanty, P., Kapoor, U., Sundaravadivelu Devarajan, D., Phan, T.M., Rizuan, A. and Mittal, J. (2022). Principles governing the phase separation of multidomain proteins. *Biochemistry* 61, 2443–2455. 10.1021/acs.biochem.2c00210.
13. Pak, C.W., Kosno, M., Holehouse, A.S., Padrick, S.B., Mittal, A., Ali, R., Yunus, A.A., Liu, D.R., Pappu, R. V. and Rosen, M.K. (2016). Sequence determinants of intracellular phase separation by complex coacervation of a disordered protein. *Mol. Cell* 63, 72–85. 10.1016/j.molcel.2016.05.042.
14. King, M.R., Lin, A.Z., Ruff, K.M., Farag, M., Ouyang, W., Vahey, M.D., Lundberg, E. and Pappu, R. V. (2022). Uncovering molecular grammars of intrinsically disordered regions that organize nucleolar fibrillar centers. *bioRxiv* 2022.11.05.515292.
15. Vernon, R.M., Andrew Chong, P., Tsang, B., Hun Kim, T., Bah, A., Farber, P., Lin, H., and Forman-Kay, J.D. (2018). Pi-pi contacts are an overlooked protein feature relevant to phase separation. *eLife* 7, e31486. 10.7554/eLife.31486.
16. Wang, J., Choi, J.M., Holehouse, A.S., Lee, H.O., Zhang, X., Jahnel, M., Maharana, S., Lemaître, R., Pozniakovskiy, A., Drechsel, D., et al. (2018). A Molecular grammar governing the driving forces for phase separation of prion-like RNA binding proteins. *Cell* 174, 688–699. 10.1016/j.cell.2018.06.006.

17. Spegg, V. and Altmeyer, M. (2021). Biomolecular condensates at sites of DNA damage: more than just a phase. *DNA Repair (Amst)*. *106*, 103179. 10.1016/j.dnarep.2021.103179.
18. Sing, C. E. and Perry, S. L. (2020). Recent progress in the science of complex coacervation. *Soft Matter* *16*, 2885–2914. 10.1039/d0sm00001a.
19. Greig, J.A., Nguyen, T.A., Lee, M., Holehouse, A.S., Posey, A.E., Pappu, R. V. and Jedd, G. (2020). Arginine-enriched mixed-charge domains provide cohesion for nuclear speckle condensation. *Mol. Cell* *77*, 1237–1250. 10.1016/j.molcel.2020.01.025.
20. Pappu, R. V., Cohen, S. R., Dar, F., Farag, M. and Kar, M. (2023). Phase transitions of associative biomacromolecules. *Chem. Rev.* *123*, 8945–8987. 10.1021/acs.chemrev.2c00814.
21. Dinic, J., Marciel, A. B. and Tirrell, M. V. (2021). Polyampholyte physics: Liquid–liquid phase separation and biological condensates. *Curr. Opin. Colloid Interface Sci.* *54*, 101457. 10.1016/j.cocis.2021.101457.
22. Mittag, T. and Pappu, R. V. (2022). A conceptual framework for understanding phase separation and addressing open questions and challenges. *Mol. Cell* *82*, 2201–2214. 10.1016/j.molcel.2022.05.018.
23. Mohan, A., Oldfield, C.J., Radivojac, P., Vacic, V., Cortese, M.S., Dunker, A.K. and Uversky, V.N. (2006). Analysis of molecular recognition features (MoRFs). *J. Mol. Biol.* *362*, 1043–1059. 10.1016/j.jmb.2006.07.087.
24. Semenov, A. N. and Rubinstein, M. (1998). Thermoreversible gelation in solutions of associative polymers. 1. Statics. *Macromolecules* *31*, 1373–1385. 10.1021/ma970616h.
25. Bremer, A., Farag, M., Borchers, W.M., Peran, I., Martin, E.W., Pappu, R. V. and Mittag, T. (2021). Deciphering how naturally occurring sequence features impact the phase behaviours of disordered prion-like domains. *Nat. Chem.* *14*, 196–207. 10.1038/s41557-021-00840-w.
26. Choi, J. M., Holehouse, A. S. and Pappu, R. V. (2020). Physical principles underlying the complex biology of intracellular phase transitions. *Annu. Rev. Biophys.* *49*, 107–133. 10.1146/annurev-biophys-121219-081629.
27. Cohan, M. C., Shinn, M. K., Lalmansingh, J. M. and Pappu, R. V. (2022). Uncovering non-random binary patterns within sequences of intrinsically disordered proteins. *J. Mol. Biol.* *434*, 167373. 10.1016/j.jmb.2021.167373.
28. Zarin, T., Strome, B., Peng, G., Pritišanac, I., Forman-Kay, J.D. and Moses, A.M. (2021). Identifying molecular features that are associated with biological function of intrinsically disordered protein regions. *eLife* *10*, 1–36. 10.7554/eLife.60220.
29. Ruff, K.M., Choi, Y.H., Cox, D., Ormsby, A.R., Myung, Y., Ascher, D.B., Radford, S.E., Pappu, R. V. and Hatters, D.M. (2022). Sequence grammar underlying unfolding and phase separation of globular proteins. *Molecular Cell* *82*, 3193–3208. 10.2139/ssrn.3929009.
30. Zhou, H. X., Nguemaha, V., Mazarakos, K. and Qin, S. (2018). Why do disordered and structured proteins behave differently in phase separation? *Trends Biochem. Sci.* *43*, 499–516. 10.1016/j.tibs.2018.03.007.
31. Banjade, S., Wu, Q., Mittal, A., Peeples, W.B., Pappu, R. V. and Rosen, M.K. (2015). Conserved interdomain linker promotes phase separation of the multivalent adaptor protein Nck. *Proc. Natl. Acad. Sci. USA* *112*, e6426–e6435. 10.1073/pnas.1508778112.
32. Martínez-Fábregas, J., Díaz-Moreno, I., González-Arzola, K., Janochas, S., Navarro, J.A., Hervás, M., Bernhardt, R., Velázquez-Campoy, A., Díaz-Quintana, A. and De la Rosa, M.A. (2014). Structural and functional analysis of novel human cytochrome c targets in apoptosis. *Mol. Cell. Proteomics* *13*, 1439–1456. 10.1074/mcp.M113.034322.

33. Martínez-Fábregas, J., Díaz-Moreno, I., González-Arzola, K., Díaz-Quintana, A. and De la Rosa, M.A. (2014). A common signalosome for programmed cell death in humans and plants. *Cell Death Dis.* 5, e1314. 10.1038/cddis.2014.280.
34. González-Arzola, K., Díaz-Quintana, A., Bernardo-García, N., Martínez-Fábregas, J., Rivero-Rodríguez, F., Casado-Combreras, M.Á., Elena-Real, C.A., Velázquez-Cruz, A., Gil-Caballero, S., Velázquez-Campoy, A., et al. (2022). Nucleus-translocated mitochondrial cytochrome *c* liberates nucleophosmin-sequestered ARF tumor suppressor by changing nucleolar liquid-liquid phase separation. *Nat. Struct. Mol. Biol.* 29, 1024–1036. 10.1038/s41594-022-00842-3.
35. Martelli, F., Hamilton, T., Silver, D.P., Sharpless, N.E., Bardeesy, N., Rokas, M., DePinho, R.A., Livingston, D.M. and Grossman, S.R. (2001). p19ARF targets certain E2F species for degradation. *Proc. Natl. Acad. Sci. USA* 98, 4455. 10.1073/pnas.081061398.
36. Okuwaki, M. and Nagata, K. (1998). Template activating factor-I remodels the chromatin structure and stimulates transcription from the chromatin template. *J. Biol. Chem.* 273, 34511–34518. 10.1074/jbc.273.51.34511.
37. Estanyol, J.M., Jaumot, M., Casanovas, O., Rodríguez-Vilarrupla, A., Agell, N. and Bachs, O. (1999). The protein SET regulates the inhibitory effect of p21(Cip1) on cyclin E-cyclin-dependent kinase 2 activity. *J. Biol. Chem.* 274, 33161–33165. 10.1074/jbc.274.46.33161.
38. Fan, Z., Beresford, P. J., Oh, D. Y., Zhang, D. and Lieberman, J. (2003). Tumor suppressor NM23-H1 is a Granzyme A-activated DNase during CTL-mediated apoptosis, and the nucleosome assembly protein SET is its inhibitor. *Cell* 112, 659–672. 10.1016/s0092-8674(03)00150-8.
39. Muto, S., Senda, M., Akai, Y., Sato, L., Suzuki, T., Nagai, R., Senda, T. and Horikoshi, M. (2007). Relationship between the structure of SET/TAF-I β /INHAT and its histone chaperone activity. *Proc. Natl. Acad. Sci.* 104, 4285–4290. 10.1073/pnas.0603762104.
40. Kato, K., Okuwaki, M. and Nagata, K. (2011). Role of Template Activating Factor-I as a chaperone in linker histone dynamics. *J. Cell Sci.* 124, 3254–3265. 10.1242/jcs.083139.
41. Kalousi, A., Hoffbeck, A.S., Selemenakis, P.N., Pinder, J., Savage, K.I., Khanna, K.K., Brino, L., Dellaire, G., Gorgoulis, V.G. and Soutoglou, E. (2015). The nuclear oncogene SET controls DNA repair by KAP1 and HP1 retention to chromatin. *Cell Rep.* 11, 149–163. 10.1016/j.celrep.2015.03.005.
42. Mandemaker, I.K., Zhou, D., Bruens, S.T., Dekkers, D.H., Verschure, P.J., Edupuganti, R.R., Meshorer, E., Demmer, J.A. and Marteijn, J.A. (2020). Histone H1 eviction by the histone chaperone SET reduces cell survival following DNA damage. *J. Cell Sci.* 133, jcs235473. 10.1242/jcs.235473.
43. González-Arzola, K., Díaz-Moreno, I., Cano-González, A., Díaz-Quintana, A., Velázquez-Campoy, A., Moreno-Beltrán, B., López-Rivas, A., and De la Rosa, M.A. (2015). Structural basis for inhibition of the histone chaperone activity of SET/TAF-I β by cytochrome *c*. *Proc. Natl. Acad. Sci.* 112, 9908–9913. 10.1073/pnas.1508040112.
44. Casado-Combreras, M.Á., Rivero-Rodríguez, F., Elena-Real, C.A., Molodenskiy, D., Díaz-Quintana, A., Martinho, M., Gerbaud, G., González-Arzola, K., Velázquez-Campoy, A., Svergun, D., et al. (2022). PP2A is activated by cytochrome *c* upon formation of a diffuse encounter complex with SET/TAF-I β . *Comput. Struct. Biotechnol. J.* 20, 3695–3707. 10.1016/j.csbj.2022.07.009.
45. Li, M., Makkinje, A. and Damuni, Z. (1996). The myeloid leukemia-associated protein SET is a potent inhibitor of protein phosphatase 2A. *J. Biol. Chem.* 271, 11059–11062. 10.1074/jbc.271.19.11059.
46. Altmeyer, M., Neelsen, K.J., Teloni, F., Pozdnyakova, I., Pellegrino, S., Grøfte, M., Rask, M.B.D., Streicher, W., Jungmichel, S., Nielsen, M.L., et al. (2015). Liquid demixing of

- intrinsically disordered proteins is seeded by poly(ADP-ribose). *Nat. Commun.* 6, 8088. 10.1038/ncomms9088.
47. Kilic, S., Lezaja, A., Gatti, M., Bianco, E., Michelena, J., Imhof, R. and Altmeyer, M. (2019). Phase separation of 53BP1 determines liquid-like behavior of DNA repair compartments. *EMBO J.* 38, e101379. 10.15252/embj.2018101379.
 48. Larson, A.G., Elnatan, D., Keenen, M.M., Trnka, M.J., Johnston, J.B., Burlingame, A.L., Agard, D.A., Redding, S. and Narlikar, G.J. (2017). Liquid droplet formation by HP1 α suggests a role for phase separation in heterochromatin. *Nature* 547, 236–240. 10.1038/nature22822.
 49. Sanulli, S., Trnka, M.J., Dharmarajan, V., Tibble, R.W., Pascal, B.D., Burlingame, A.L., Griffin, P.R., Gross, J.D. and Narlikar, G.J. (2019). HP1 reshapes nucleosome core to promote phase separation of heterochromatin. *Nature* 575, 390–394. 10.1038/s41586-019-1669-2.
 50. Karetsov, Z., Emmanouilidou, A., Sanidas, I., Liokatis, S., Nikolakaki, E., Politou, A.S. and Papamarcaki, T. (2009). Identification of distinct SET/TAF-I β domains required for core histone binding and quantitative characterisation of the interaction. *BMC Biochem.* 10, 10. 10.1186/1471-2091-10-10.
 51. Box, J.K., Paquet, N., Adams, M.N., Boucher, D., Bolderson, E., O'Byrne, K.J. and Richard, D.J. (2016). Nucleophosmin: from structure and function to disease development. *BMC Mol. Biol.* 17, 19. 10.1186/s12867-016-0073-9.
 52. Banani, S.F., Rice, A.M., Peeples, W.B., Lin, Y., Jain, S., Parker, R. and Rosen, M.K. (2016). Compositional control of phase-separated cellular bodies. *Cell* 166, 651–663. 10.1016/j.cell.2016.06.010.
 53. Feric, M., Vaidya, N., Harmon, T.S., Mitrea, D.M., Zhu, L., Richardson, T.M., Kriwacki, R.W., Pappu, R. V. and Brangwynne, C.P. (2016). Coexisting liquid phases underlie nucleolar subcompartments. *Cell* 165, 1686–1697. 10.1016/j.cell.2016.04.047.
 54. Mitrea, D.M., Cika, J.A., Guy, C.S., Ban, D., Banerjee, P.R., Stanley, C.B., Nourse, A., Deniz, A.A. and Kriwacki, R.W. (2016). Nucleophosmin integrates within the nucleolus via multi-modal interactions with proteins displaying R-rich linear motifs and rRNA. *eLife* 5, 1–33. 10.7554/elife.13571.
 55. Mitrea, D.M., Grace, C.R., Buljan, M., Yun, M.K., Pytel, N.J., Satumba, J., Nourse, A., Park, C.G., Babu, M.M., White, S.W., et al. (2014). Structural polymorphism in the N-terminal oligomerization domain of NPM1. *Proc. Natl. Acad. Sci. USA* 111, 4466–4471. 10.1073/pnas.1321007111.
 56. Mitrea, D.M., Cika, J.A., Stanley, C.B., Nourse, A., Onuchic, P.L., Banerjee, P.R., Phillips, A.H., Park, C.G., Deniz, A.A. and Kriwacki, R.W. (2018). Self-interaction of NPM1 modulates multiple mechanisms of liquid-liquid phase separation. *Nat. Commun.* 9, 1–13. 10.1038/s41467-018-03255-3.
 57. Mitrea D.M. and Kriwacki R.W. (2018). On the relationship status for Arf and NPM1 - it's complicated. *FEBS J.* 285, 828–831. 10.1111/febs.14407.
 58. Capaldi, R. A., Darley-Usmar, V., Fuller, S. and Millett, F. (1982). Structural and functional features of the interaction of cytochrome c with complex III and cytochrome c oxidase. *FEBS Lett.* 138, 1–7. 10.1016/0014-5793(82)80382-7.
 59. Navarro, J. A., Hervás, M., Genzor, C. G., Cheddar, G., Fillat, M. F., De la Rosa, M. A., Gómez-Moreno, C., Cheng, H., Xia, B., Chae, Y. K. et al. (1995). Site-specific mutagenesis demonstrates that the structural requirements for efficient electron transfer in *Anabaena* ferredoxin and flavodoxin are highly dependent on the reaction partner: kinetic studies with photosystem I, ferredoxin:NADP⁺ reductase, and cytochrome c. *Arch. Biochem. Biophys.* 321, 229–238. 10.1006/abbi.1995.1390.
 60. Kurki, S., Peltonen, K., Latonen, L., Kiviharju, T.M., Ojala, P.M., Meek, D. and Laiho, M.

- (2004). Nucleolar protein NPM interacts with HDM2 and protects tumor suppressor protein p53 from HDM2-mediated degradation. *Cancer Cell* 5, 465–475. 10.1016/s1535-6108(04)00110-2.
61. Jones, S., Holm, T., Mäger, I., Langel, Ü. and Howl, J. (2010). Characterization of bioactive cell penetrating peptides from human cytochrome c: Protein mimicry and the development of a novel apoptogenic agent. *Chem. Biol.* 17, 735–744. 10.1016/j.chembiol.2010.05.018.
 62. Levone, B.R., Lenzken, S.C., Antonaci, M., Maiser, A., Rapp, A., Conte, F., Reber, S., Mechttersheimer, J., Ronchi, A.E., Mühlemann, O. et al. (2021). FUS-dependent liquid-liquid phase separation is important for DNA repair initiation. *J. Cell Biol.* 220, e202008030. 10.1083/jcb.202008030.
 63. Gracia, P., Polanco, D., Tarancón-Díez, J., Serra, I., Bracci, M., Oroz, J., Laurents, D. V., García, I. and Cremades, N. (2022). Molecular mechanism for the synchronized electrostatic coacervation and co-aggregation of alpha-synuclein and tau. *Nat. Commun.* 13, 4586. 10.1038/s41467-022-32350-9.
 64. Molliex, A., Temirov, J., Lee, J., Coughlin, M., Kanagaraj, A.P., Kim, H.J., Mittag, T. and Taylor, J.P. (2015). Phase separation by low complexity domains promotes stress granule assembly and drives pathological fibrillization. *Cell* 163, 123–133. 10.1016/j.cell.2015.09.015.
 65. Fossat, M. J., Zeng, X. and Pappu, R. V. (2021). Uncovering differences in hydration free energies and structures for model compound mimics of charged side chains of amino acids. *J. Phys. Chem. B* 125, 4148–4161. 10.1021/acs.jpcc.1c01073.
 66. Zeng, X., Ruff, K. M. and Pappu, R. V. (2022). Competing interactions give rise to two-state behavior and switch-like transitions in charge-rich intrinsically disordered proteins. *Proc. Natl. Acad. Sci. USA* 119, 1–10. 10.1073/pnas.2200559119.
 67. Ukmar-Godec, T., Hutten, S., Grieshop, M.P., Rezaei-Ghaleh, N., Cima-Omori, M.S., Biernat, J., Mandelkow, E., Söding, J., Dormann, D. and Zweckstetter, M. (2019). Lysine/RNA-interactions drive and regulate biomolecular condensation. *Nat. Commun.* 10, 1–15. 10.1038/s41467-019-10792-y.
 68. Cooper, A. (2005). Heat capacity effects in protein folding and ligand binding: a re-evaluation of the role of water in biomolecular thermodynamics. *Biophys. Chem.* 115, 89–97. 10.1016/j.bpc.2004.12.011.
 69. Pylaeva, S., Brehm, M. and Sebastiani, D. (2018). Salt bridge in aqueous solution: strong structural motifs but weak enthalpic effect. *Sci. Rep.* 8, 1–7. 10.1038/s41598-018-31935-z.
 70. Cho, B., Choi, J., Kim, R., Yun, J.N., Choi, Y., Lee, H.H. and Koh, J. (2021). Thermodynamic models for assembly of intrinsically disordered protein hubs with multiple interaction partners. *J. Am. Chem. Soc.* 143, 12509–12523. 10.1021/jacs.1c00811.
 71. Mukherjee, S. and Schäfer, L.V. (2023). Thermodynamic forces from protein and water govern condensate formation of an intrinsically disordered protein domain. *Nat. Commun.* 14, 5892. 10.1038/s41467-023-41586-y
 72. Mollica, L., Bessa, L.M., Hanouille, X., Jensen, M.R., Blackledge, M. and Schneider, R. (2016). Binding mechanisms of intrinsically disordered proteins: Theory, simulation, and experiment. *Frontiers in Molecular Biosciences* 3, 52. 10.3389/fmolb.2016.00052.
 73. Falahati, H. and Haji-Akbari, A. (2019). Thermodynamically driven assemblies and liquid-liquid phase separations in biology. *Soft Matter* 15, 1135–1154. 10.1039/c8sm02285b.
 74. Guseva S., Schnapka V., Adamski W., Maurin D., Ruigrok R.W.H., Salvi N. and Blackledge M. (2023). Liquid–liquid phase separation modifies the dynamic properties of intrinsically disordered proteins. *J. Am. Chem. Soc.* 145, 10548–10563. 10.1021/jacs.2c13647.

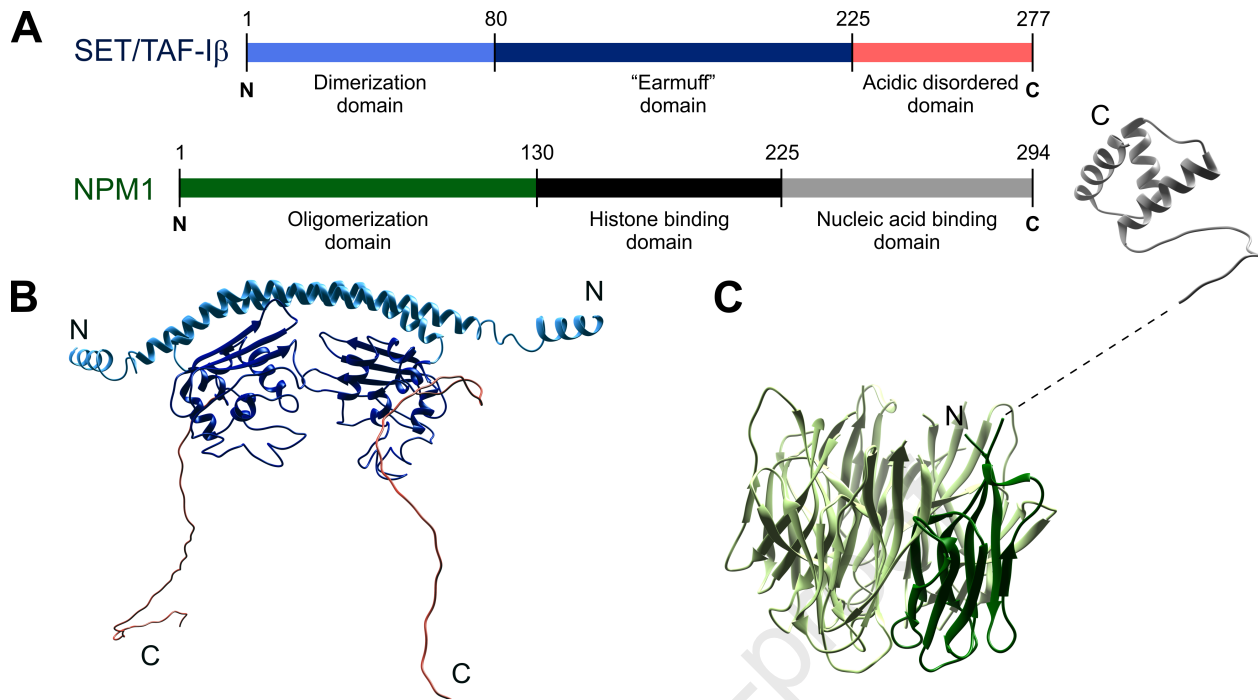
75. Banci, L., Bertini, I., De la Rosa, M. A., Koulougliotis, D., Navarro, J.A. and Walter, O. (1998). Solution structure of oxidized cytochrome c_6 from the green alga *Monoraphidium braunii*. *Biochemistry*. 37, 4831–4843. 10.1021/bi972765y.
76. Blauer, G., Sreerama, N. and Woody, R. W. (1993). Optical activity of hemoproteins in the Soret region. Circular dichroism of the heme undecapeptide of cytochrome *c* in aqueous solution. *Biochemistry* 32, 6674–6679. 10.1021/bi00077a021.
77. Navarro, J. A., Hervás, M., De la Cerda, B. and De la Rosa, M.A. (1995). Purification and physicochemical properties of the low-potential cytochrome c_{549} from the cyanobacterium *Synechocystis* sp. PCC 6803. *Arch. Biochem. Biophys.* 318, 46–52. 10.1006/abbi.1995.1202.
78. Díaz, A., Navarro, F., Hervás, M., Navarro, J. A., Chávez, S., Florencio, F. J. and De la Rosa, M.A. (1994). Cloning and correct expression in *E. coli* of the *petJ* gene encoding cytochrome c_6 from *Synechocystis* 6803. *FEBS Lett.* 347, 173–177. 10.1016/0014-5793(94)00529-x.
79. Fitch, C. A., Platzer, G., Okon, M., Garcia-Moreno, B. E. and McIntosh, L. P. (2015). Arginine: its pKa value revisited. *Protein Sci.* 24, 752–761. 10.1002/pro.2647.
80. Gobbi, A. and Frenking, G. (1993). Y-conjugated compounds: the equilibrium geometries and electronic structures of guanidine, guanidinium cation, urea, and 1,1-diaminoethylene. *J. Am. Chem. Soc.* 115, 2362–2372. 10.1021/ja00059a035.
81. Alberti, S., Saha, S., Woodruff, J.B., Franzmann, T.M., Wang, J. and Hyman, A.A. (2018). A user's guide for phase separation assays with purified proteins. *J. Mol. Biol.* 430, 4806–4820. 10.1016/j.jmb.2018.06.038.
82. Ray, S., Singh, N., Patel, K., Krishnamoorthy, G. and Maji, S. K. (2023). FRAP and FRET investigation of α -synuclein fibrillization via liquid-liquid phase separation *in vitro* and in HeLa cells. *Methods Mol. Biol.* 2551, 395–423. 10.1007/978-1-0716-2597-2_26.
83. Shiina, N. (2019). Liquid- and solid-like RNA granules form through specific scaffold proteins and combine into biphasic granules. *J. Biol. Chem.* 294, 3532–3548. 10.1074/jbc.RA118.005423.
84. Patel, A., Lee, H.O., Jawerth, L., Drechsel, D., Hyman, A.A., Alberti, S., Maharana, S., Jahnel, M., Hein, M.Y., Stoykov, S., et al. (2015). A liquid-to-solid phase transition of the ALS protein FUS accelerated by disease mutation. *Cell* 162, 1066–1077. 10.1016/j.cell.2015.07.047.
85. Xu B., He G., Weiner B.G., Ronceray P., Meir Y., Jonikas M.C. and Wingreen N.S. (2020). Rigidity enhances a magic-number effect in polymer phase separation. *Nat Commun.* 11, 1561. 10.1038/s41467-020-15395-6.
86. Ahn, J. II, Park, J.-E., Meng, L., Zhang, L., Kim, T.-S., Kruhlak, M.J., Kim, B.Y. and Lee, K.S. (2020). Phase separation of the Cep63•Cep152 complex underlies the formation of dynamic supramolecular self-assemblies at human centrosomes. *Cell Cycle* 19, 3437–3457. 10.1080/15384101.2020.1843777.
87. Sabari, B. R., Dall'Agnese, A. and Young R. A. (2020). Biomolecular condensates in the nucleus. *Trends Biochem Sci* 45, Issue 11, 961–977. 10.1016/j.tibs.2020.06.007.
88. Singatulina, A.S., Hamon, L., Sukhanova, M.V., Desforges, B., Joshi, V., Bouhss, A., Lavrik, O. I., Paste, D. (2019) PARP-1 activation directs FUS to DNA damage sites to form PARG-reversible compartments enriched in damaged DNA. *Cell Rep* 27, 1809–1821. 10.1016/j.celrep.2019.04.031
89. Zgheib, O., Pataky, K., Brugger, J. and Halazonetis T.D. (2008) An oligomerized 53BP1 tudor domain suffices for recognition of DNA double-strand breaks. *Mol Cell Biol* 29, 1050–1058. 10.1128/MCB.01011-08.
90. Mittag, T., Marsh, J., Grishaev, A., Orlicky, S., Lin, H., Sicheri, F., Tyers, M., Forman-

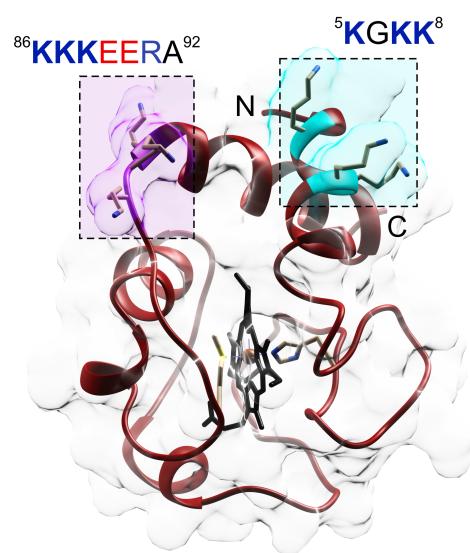
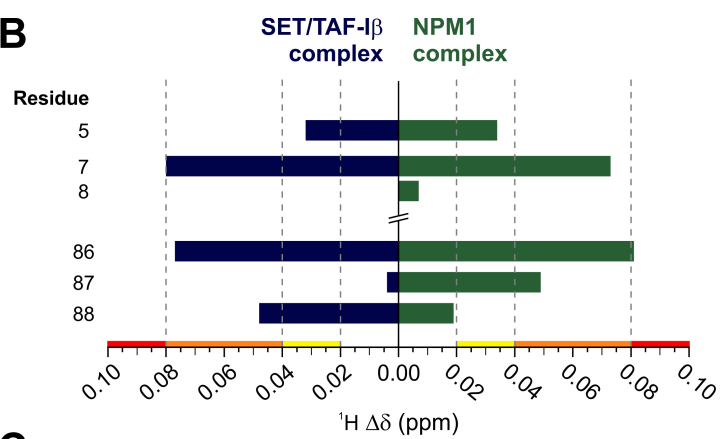
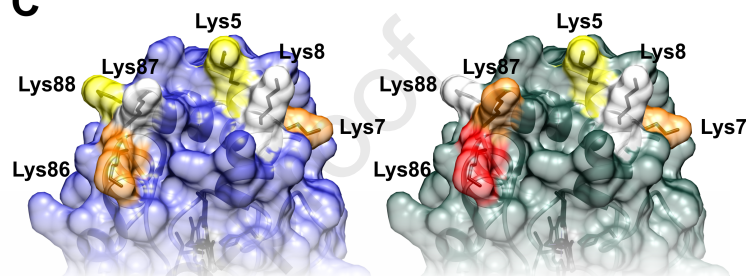
- Kay, J.D. (2010) Structure/function implications in a dynamic complex of the intrinsically disordered Sic1 with the Cdc4 subunit of an SCF ubiquitin ligase. *Structure* 18, 494–506. 10.1016/j.str.2010.01.020.
91. Rivero-Rodríguez, F., Díaz-Quintana, A., Velázquez-Cruz, A., González-Arzola, K., Gavilan, M.P., Velázquez-Campoy, A., Ríos, R.M., De la Rosa, M.A., and Díaz-Moreno I. (2021). Inhibition of the PP2A activity by the histone chaperone ANP32B is long-range allosterically regulated by respiratory cytochrome c. *Redox Biol.* 43: 101967. 10.1016/j.redox.2021.101967.
 92. Mahadevi, A. S. and Sastry, G. N. (2016). Cooperativity in noncovalent interactions. *Chem. Rev.* 116, 2775–2825. 10.1021/cr500344e.
 93. Choi, J., Hyman, A. A. and Pappu, R. V. (2020). Generalized models for bond percolation transitions of associative polymers. *Phys. Rev. E* 102, 1–6. 10.1103/PhysRevE.102.042403.
 94. Murray, D.T., Kato, M., Lin, Y., Thurber, K. R., Hung, I., McKnight, S.L. and Tycko, R. (2017) Structure of FUS protein fibrils and its relevance to self-assembly and phase separation of low-complexity domains. *Cell* 171, 615–627. 10.1016/j.cell.2017.08.048.
 95. Carlson, C. R., Asfaha, J. B., Ghent, C. M., Howard, C. J., Hartooni, N., Safari, M., Frankel, A. D. and Morgan, D. O. (2020) Phosphoregulation of phase separation by the SARS-CoV-2 N protein suggests a biophysical basis for its dual functions. *Mol Cell* 80, 1092–1103. 10.1016/j.molcel.2020.11.025.
 96. Sanulli, S., Trnka, M.J., Dharmarajan, V., Tibble, R. W., Pascal, B. D., Burlingame, A. L., Griffin, P. R., Gross, J. D. and Narlikar, G. J. (2019) HP1 reshapes nucleosome core to promote phase separation of heterochromatin. *Nature* 575, 390–394. 10.1038/s41586-019-1669-2.
 97. Buzón, P., Velázquez-Cruz, A., Corrales-Guerrero, L., Díaz-Quintana, A., Díaz-Moreno, I. and Roos, W.H. (2023). The histone chaperones SET/TAF-1 β and NPM1 exhibit conserved functionality in nucleosome remodeling and histone eviction in a cytochrome c-dependent manner. *Adv. Sci.* e2301859. 10.1002/adv.202301859.
 98. Díaz-Moreno, I., Velázquez-Cruz, A., Curran-French, S., Díaz-Quintana, A. and De la Rosa, M.A. (2018). Nuclear cytochrome c – a mitochondrial visitor regulating damaged chromatin dynamics. *FEBS Lett.* 592, 172–178. 10.1002/1873-3468.12959.
 99. Ramazi, S. and Zahiri, J. (2021). Post-translational modifications in proteins: resources, tools and prediction methods. *Database baab012*, 1–20. 10.1093/database/baab012.
 100. Kim, S.C., Sprung, R., Chen, Y., Xu, Y., Ball, H., Pei, J., Cheng, T., Kho, Y., Xiao, H., Xiao, L., et al. (2006). Substrate and functional diversity of lysine acetylation revealed by a proteomics survey. *Mol. Cell* 23, 607–618. 10.1016/j.molcel.2006.06.026.
 101. Bazylanska, V., Kalpage, H.A., Wan, J., Vaishnav, A., Mahapatra, G., Turner, A.A., Chowdhury, D.D., Kim, K., Morse, P.T., Lee, I., et al. (2021). Lysine 53 acetylation of cytochrome c in prostate cancer: Warburg metabolism and evasion of apoptosis. *Cells* 10, 802. 10.3390/cells10040802.
 102. Morse, P.T., Pérez-Mejías, G., Wan, J., Turner, A.A., Márquez, I., Kalpage, H.A., Vaishnav, A., Zurek, M.P., Huettmann, P.P., Kim, K., et al. (2023). Cytochrome c lysine acetylation regulates cellular respiration and cell death in ischemic skeletal muscle. *Nat. Commun.* 14, 4166. 10.1038/s41467-023-39820-8.
 103. Prakash, H. and Mazumdar, S. (2009). Succinylation of cytochrome c investigated by electrospray ionization mass spectrometry: reactive lysine residues. *Int. J. Mass Spectrom.* 281, 55–62. 10.1016/j.ijms.2008.12.013.
 104. Boeynaems, S., Alberti, S., Fawzi, N.L., Mittag, T., Polymenidou, M., Rousseau, F., Schymkowitz, J., Shorter, J., Wolozin, B., Van Den Bosch, L., et al. (2018). Protein phase separation: a new phase in cell biology. *Trends Cell Biol.* 28, 420–435. 10.1016/j.tcb.2018.02.004.

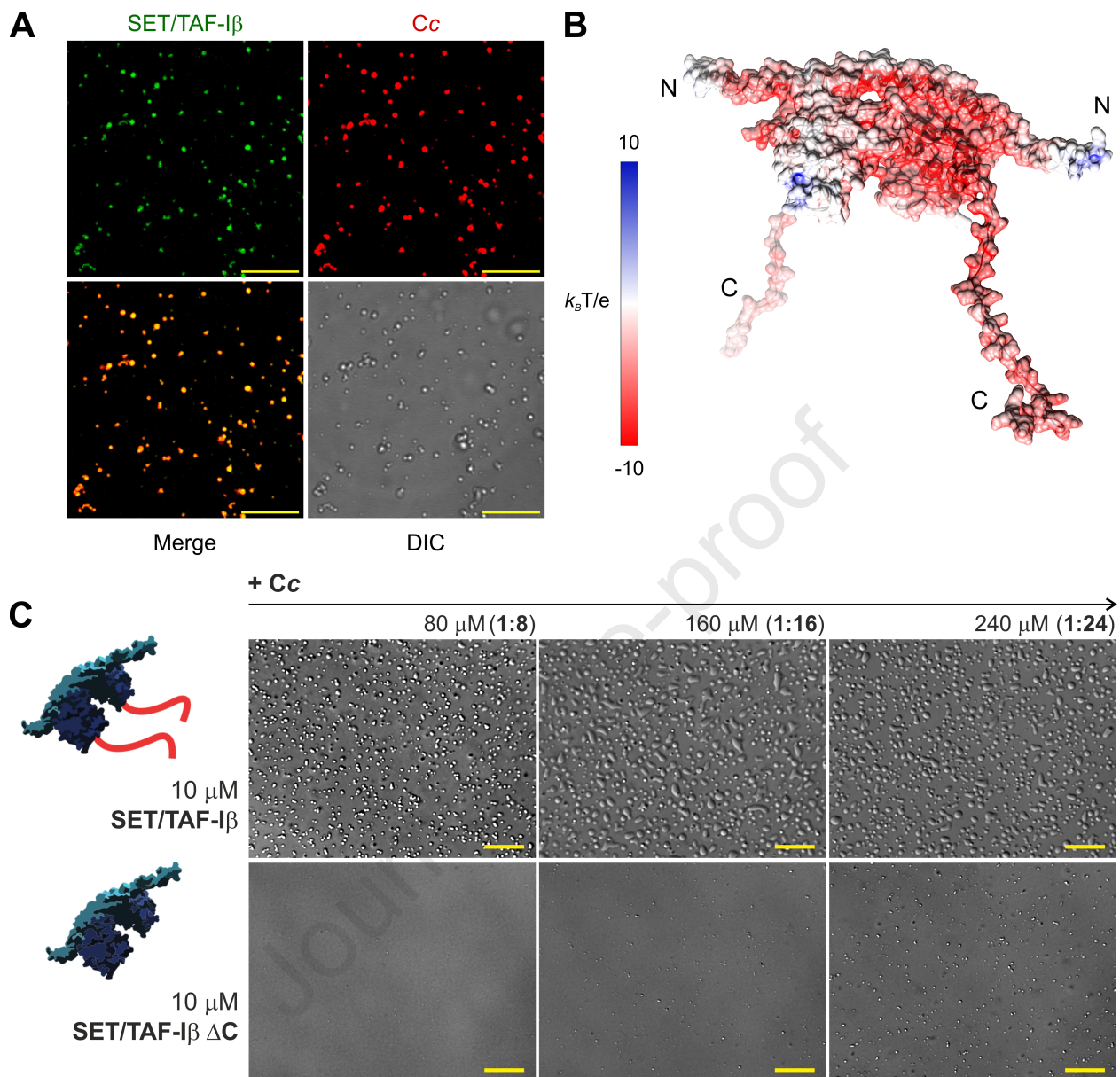
105. Webb, B. and Sali, A. (2017). Protein structure modeling with MODELLER. *Methods Mol. Biol.* *1654*, 39–54. 10.1007/978-1-4939-7231-9_4.
106. Gallo, A., Lo Sterzo, C., Mori, M., Di Matteo, A., Bertini, I., Banci, L., Brunori, M. and Federici, L. (2012). Structure of nucleophosmin DNA-binding domain and analysis of its complex with a G-quadruplex sequence from the c-MYC promoter. *J. Biol. Chem.* *287*, 26539–26548. 10.1074/jbc.m112.371013.
107. Imai, M., Saio, T., Kumeta, H., Uchida, T., Inagaki, F. and Ishimori, K. (2016). Investigation of the redox-dependent modulation of structure and dynamics in human cytochrome *c*. *Biochem. Biophys. Res. Commun.* *469*, 978–984. 10.1016/j.bbrc.2015.12.079.
108. Olteanu, A., Patel, C.N., Dedmon, M.M., Kennedy, S., Linhoff, M.W., Minder, C.M., Potts, P.R., Deshmukh, M. and Pielak, G.J. (2003). Stability and apoptotic activity of recombinant human cytochrome *c*. *Biochem. Biophys. Res. Commun.* *312*, 733–740. 10.1016/j.bbrc.2003.10.182.
109. Pecina, P., Borisenko, G.G., Belikova, N.A., Tyurina, Y.Y., Pecinova, A., Lee, I., Samhan-Arias, A.K., Przyklenk, K., Kagan, V.E. and Hüttemann, M. (2010). Phosphomimetic substitution of cytochrome *c* tyrosine 48 decreases respiration and binding to cardiolipin and abolishes ability to trigger downstream caspase activation. *Biochemistry* *49*, 6705–6714. 10.1021/bi100486s.
110. Moreno-Beltrán, B., Díaz-Moreno, I., González-Arzola, K., Guerra-Castellano, A., Velázquez-Campoy, A., De La Rosa, M.A. and Díaz-Quintana, A. (2015). Respiratory complexes III and IV can each bind two molecules of cytochrome *c* at low ionic strength. *FEBS Lett.* *589*, 476–483. 10.1016/j.febslet.2015.01.004.
111. Bradford, M. M. (1976). A rapid and sensitive method for the quantitation of microgram quantities of protein utilizing the principle of protein-dye binding. *Anal. Biochem.* *72*, 248–254. 10.1006/abio.1976.9999.
112. Roumestand, C. and Canet, D. (2000). Extending the excitation sculpting concept for selective excitation. *J. Magn. Reson.* *147*, 331–339. 10.1006/jmre.2000.2206.
113. Eastman, P., Swails, J., Chodera, J.D., McGibbon, R.T., Zhao, Y., Beauchamp, K.A., Wang, L.-P., Simmonett, A.C., Harrigan, M.P., Stern, C.D., et al. (2017). OpenMM 7: Rapid development of high performance algorithms for molecular dynamics. *PLOS Comput. Biol.* *13*, e1005659. 10.1371/journal.pcbi.1005659.
114. Case, D., Betz, R., Cerutti, D., Cheatham III, T., Darden, T., Duke, R., Giese, T., Gohlke, H., Goetz, A., Homeyer, N., et al. AMBER 2016. University of California, San Francisco.
115. Tian, C., Kasavajhala, K., Belfon, K.A.A., Raguette, L., Huang, H., Miguez, A.N., Bickel, J., Wang, Y., Pincay, J., Wu, Q., et al. (2020). ff19SB: Amino-acid-specific protein backbone parameters trained against quantum mechanics energy surfaces in solution. *J. Chem. Theory Comput.* *16*, 528–552. 10.1021/acs.jctc.9b00591.
116. Autenrieth, F., Tajkhorshid, E., Baudry, J. and Luthey-Schulten, Z. (2004). Classical force field parameters for the heme prosthetic group of cytochrome *c*. *J. Comput. Chem.* *25*, 1613–1622. 10.1002/jcc.20079.
117. Izadi, S., Anandakrishnan, R. and Onufriev, A. V. (2014). Building water models: a different approach. *J. Phys. Chem. Lett.* *5*, 3863–3871. 10.1021/jz501780a.
118. Andersen, H. C. (1980). Molecular dynamics simulations at constant pressure and/or temperature. *J. Chem. Phys.* *72*, 2384. 10.1063/1.439486.
119. Roe, D. R. and Cheatham, T. E. (2013). PTRAJ and CPPTRAJ: software for processing and analysis of molecular dynamics trajectory data. *J. Chem. Theory Comput.* *9*, 3084–3095. 10.1021/ct400341p.
120. Pettersen, E.F., Goddard, T.D., Huang, C.C., Couch, G.S., Greenblatt, D.M., Meng, E.C. and Ferrin, T.E. (2004). UCSF Chimera - a visualization system for exploratory research

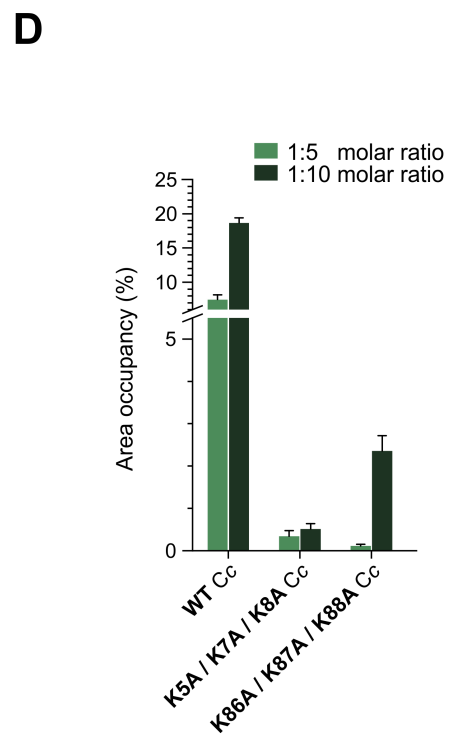
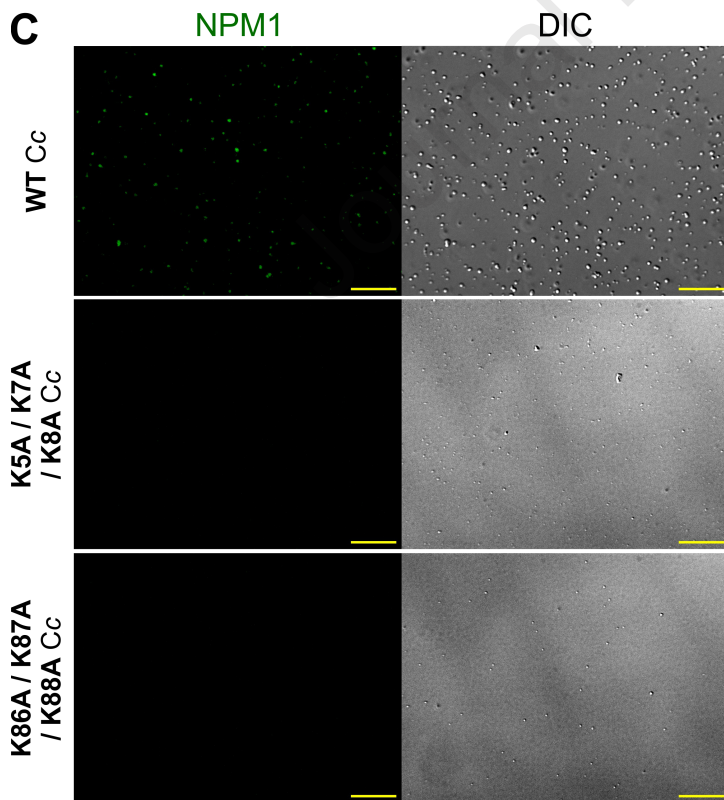
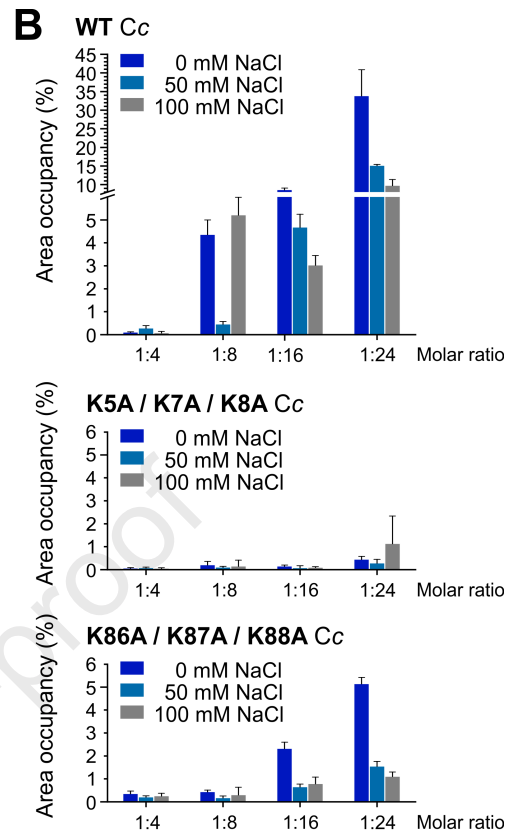
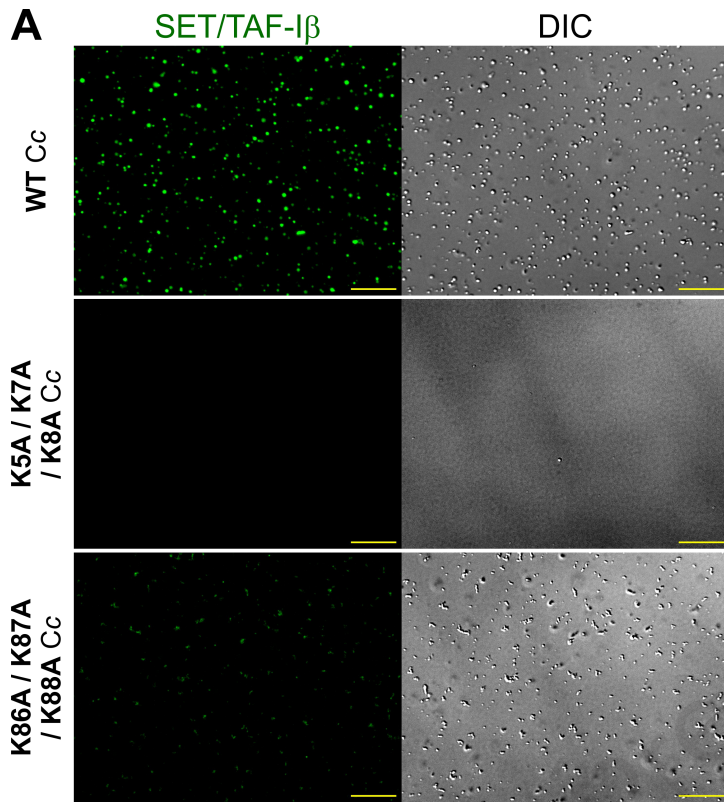
- and analysis. *J. Comput. Chem.* 25, 1605–1612. 10.1002/jcc.20084.
121. Jurrus, E., Engel, D., Star, K., Monson, K., Brandi, J., Felberg, L.E., Brookes, D.H., Wilson, L., Chen, J., Liles, K., et al. (2018). Improvements to the APBS biomolecular solvation software suite. *Protein Sci.* 27, 112–128. 10.1002/pro.3280.
 122. Dolinsky, T. J., Nielsen, J. E., McCammon, J. A. and Baker, N. A. (2004). PDB2PQR: an automated pipeline for the setup of Poisson-Boltzmann electrostatics calculations. *Nucleic Acids Res.* 32, W665–W667. 10.1093/nar/gkh381.
 123. Schindelin, J., Arganda-Carreras, I., Frise, E., Kaynig, V., Longair, M., Pietzsch, T., Preibisch, S., Rueden, C., Saalfeld, S., Schmid, B., et al. (2012). Fiji: An open-source platform for biological-image analysis. *Nat. Methods* 9, 676–682. 10.1038/nmeth.2019.

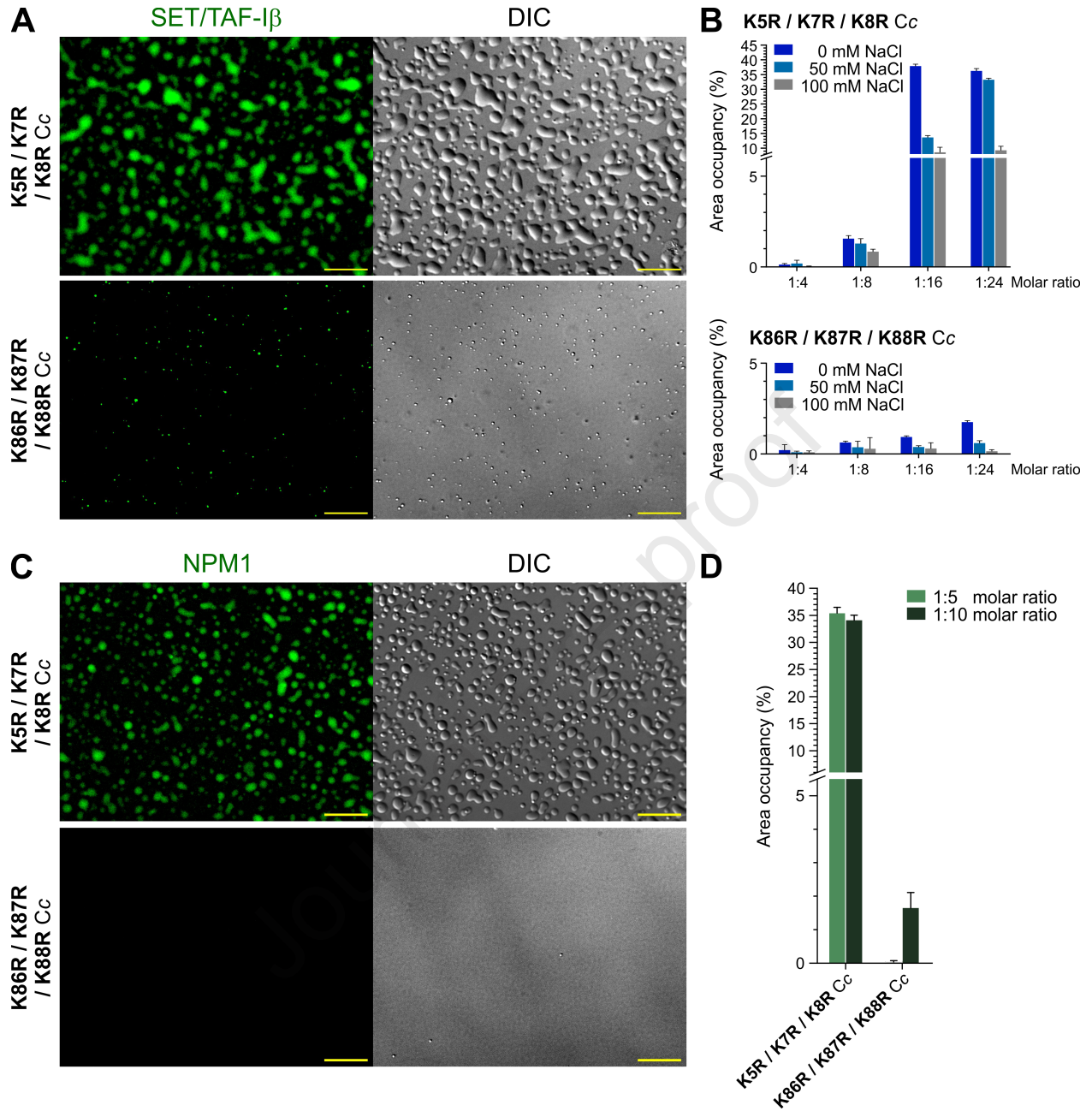
Journal Pre-proof

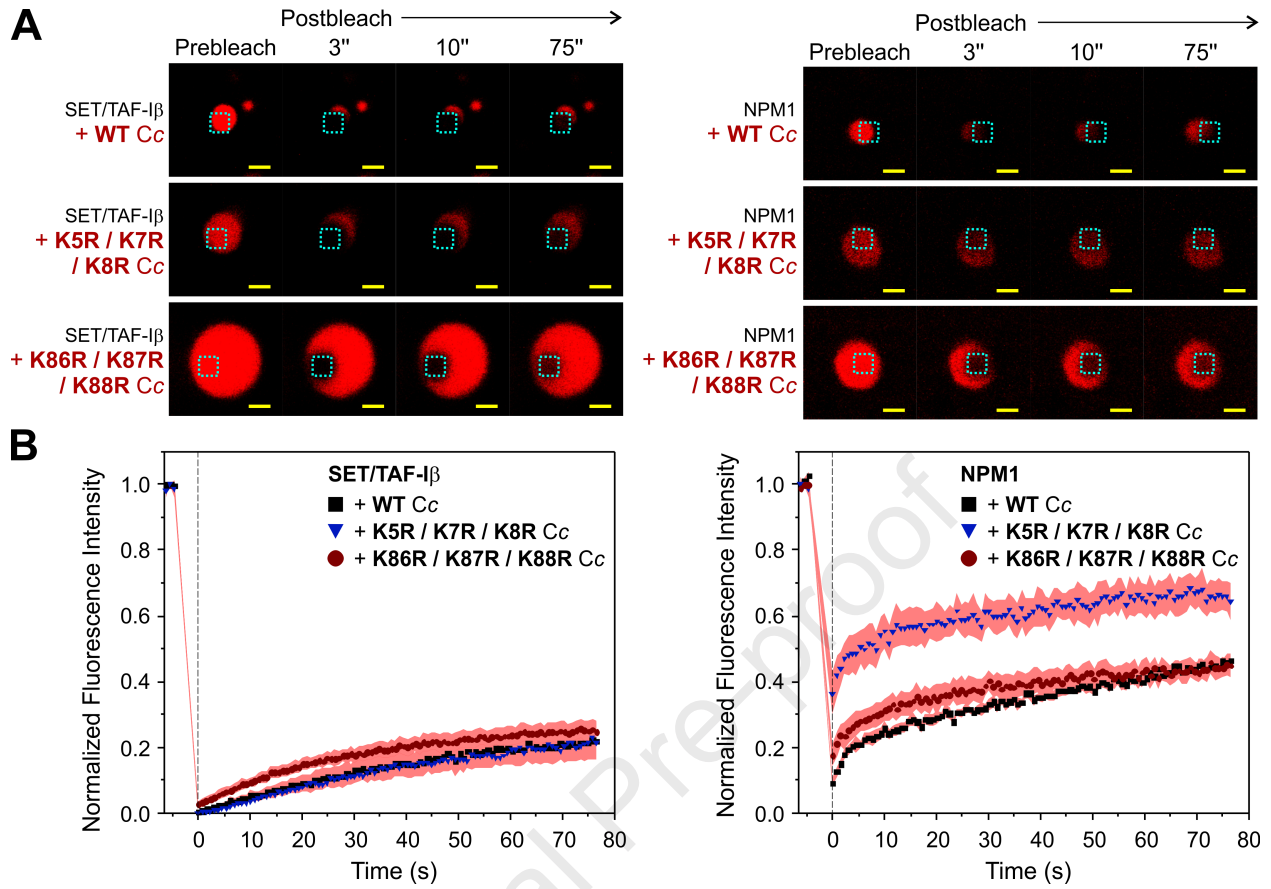


A**B****C**









Highlights

- Cytochrome *c* and SET/TAF-I β phase separate together.
- Cytochrome *c* is a protein with sequence-encoded phase-separation properties.
- Cytochrome *c*-driven dynamical rearrangement of SET/TAF-I β drives phase transition.
- Selective cytochrome *c*-mobility inside condensates harbouring SET/TAF-I β or NPM1

Journal Pre-proof

KEY RESOURCES TABLE

TABLE FOR AUTHOR TO COMPLETE

Please do not add custom subheadings. If you wish to make an entry that does not fall into one of the subheadings below, please contact your handling editor or add it under the “other” subheading. **Any subheadings not relevant to your study can be skipped.** (NOTE: references should be in numbered style, e.g., Smith et al.¹)

Key resources table

REAGENT or RESOURCE	SOURCE	IDENTIFIER
Bacterial and virus strains		
<i>Escherichia coli</i> DH5 α	Homemade	N/A
<i>Escherichia coli</i> BL21(DE3)	Homemade	N/A
<i>Escherichia coli</i> C43(DE3)	Homemade	N/A
Chemicals, peptides, and recombinant proteins		
SET/TAF-I β	Martínez-Fábregas <i>et al.</i> (2014) ³²	https://doi.org/10.1074/mcp.M113.034322 .
SET/TAF-I β Q69C mutant	This manuscript	N/A
SET/TAF-I β D226C mutant	This manuscript	N/A
SET/TAF-I β E243C mutant	This manuscript	N/A
SET/TAF-I β D260C mutant	This manuscript	N/A
SET/TAF-I β D277C mutant	This manuscript	N/A
SET/TAF-I β Δ C	Muto <i>et al.</i> (2007) ³⁹	https://doi.org/10.1073/pnas.0603762104
SET/TAF-I β Δ C Q69C mutant	Casado-Combreras <i>et al.</i> (2022) ⁴⁴	https://doi.org/10.1016/j.csbj.2022.07.009
NPM1	González-Arzola <i>et al.</i> (2022) ³⁴	https://doi.org/10.1038/s41594-022-00842-3
Cytochrome c	Olteanu <i>et al.</i> (2003) ¹⁰⁸	https://doi.org/10.1016/j.brc.2003.10.182
Cytochrome c K5A / K7A / K8A mutant	This manuscript	N/A
Cytochrome c K5R / K7R / K8R mutant	This manuscript	N/A
Cytochrome c K86A / K87A / K88A mutant	This manuscript	N/A
Cytochrome c K86R / K87R / K88R mutant	This manuscript	N/A
MTSL ([1-oxyl-2,2,5,5-tetramethyl- δ 3-pyrroline-3-methyl] methanethiosulfonate)	Toronto Research Chemicals Inc.,	Cat. n.: TRC-O875000
Oregon Green™ 488 maleimide probe (<i>Molecular Probes</i>)	Invitrogen / ThermoFisher	Cat. n.: O6034
Texas Red™-X succinimidyl ester probe (<i>Molecular Probes</i>)	Invitrogen / ThermoFisher	Cat. n.: T20175
Ficoll ^R PM70	Cytiva	Cat. n.: 17-0310-50
OmniPur® DTT (Dithiothreitol)	CalBioChem	Cat. n.: 3870-25GM
NcoI (restriction enzyme)	New England Biolabs	Cat. n.: R0193S
BamHI-HF (restriction enzyme)	New England Biolabs	Cat. n.: R3136S
DpnI (restriction enzyme)	Roche / Merck	Cat. n.: 10642988001 / DPNI-RO
T4 DNA ligase	New England Biolabs	Cat. n.: M0202S
Dimethyl sulfoxide (DMSO)	PanReac AppliChem	Cat. n.: A3672.0100
Lysozyme	Thermo Scientific	Cat. n.: 89833
DNase I	Roche	Cat. n.: 10104159001

Phenylmethylsulphonyl fluoride (PMSF)	<i>Sigma Aldrich</i>	Cat. n.: 93482-50ML-F
cOplete™ Mini, EDTA-free	<i>Roche</i>	Cat. n.: 04693132001
<i>BioRad</i> Protein assay dye reagent concentrate	<i>BioRad</i>	Cat. n.: #5000006
Critical commercial assays		
In-Fusion™ Snap Assembly EcoDry system	<i>Takara Bio</i>	Cat. n.: 638954
KOD Hot Start DNA Polymerase	<i>Sigma Aldrich</i>	Cat. n.: 71086-5
NucleoSpin Gel and PCR Clean-Up Kit	<i>Macherey-Nagel</i>	Cat. n.: 740609.50S
GenElute™ plasmid miniprep kit	<i>Sigma Aldrich</i>	Cat. n.: PLN70-1KT
Deposited data		
SET/TAF-I β Δ C structure (XRD)	Muto <i>et al.</i> (2007) ³⁹	PDB (entry 2E50)
NPM1 ₁₋₁₃₀ structure (oligomerization domain, XRD)	Mitrea <i>et al.</i> (2014) ⁵⁵	PDB (entry 4N8M)
NPM1 ₂₂₆₋₂₉₄ structure (DNA binding domain, NMR)	Gallo <i>et al.</i> (2012) ¹⁰⁶	PDB (entry 2LLH)
Reduced human cytochrome c structure (NMR)	Imai <i>et al.</i> (2016) ¹⁰⁷	PDB (entry 2N9I)
Human cytochrome c structure (XRD)	Rajagopal <i>et al.</i> (2013) [S6]	PDB (entry 3ZCF)
HDM2 RING finger domain structure (NMR)	Kostic <i>et al.</i> (2006) [S7]	PDB (entry 2HDP)
[¹ H- ¹⁵ N] HSQC-NMR titrations of reduced cytochrome c with SET/TAF-I β	González-Arzola <i>et al.</i> (2015) ⁴³	https://doi.org/10.1073/pnas.1508040112
[¹ H- ¹⁵ N] HSQC-NMR titrations of reduced cytochrome c with NPM1	González-Arzola <i>et al.</i> (2022) ³⁴	https://doi.org/10.1038/s41594-022-00842-3
ff19SB force-field libraries	Tian <i>et al.</i> (2020) ¹¹⁵	https://ambermd.org/AmblerModels.php
Force-field parameters for the heme group	Autenrieth <i>et al.</i> (2004) ¹¹⁶	https://doi.org/10.1002/jcc.20079
Oligonucleotides		
Primers used for DNA amplification, molecular cloning and mutagenesis	This manuscript	See <i>Supplementary information</i> (Table S5)
Recombinant DNA		
K5R/K7R/K8R Cc-encoding gBlock: 5' - ATGGGCGACGTGGAAAGGGGCAGGAGGATC TTCATCATGAAATGCTCGCAGTGCCACACGG TGGAAAAAGGCGGCAAACACAAAACCGGTCC CAACCTGCACGGCCTGTTCCGGCCGCAAACG GGCCAGGCGCCGGGCTACAGCTACACGGCG GCGAACAAAAACAAAGGCATCATCTGGGGCG AAGACACGCTGATGGAATACCTCGAGAACCC GAAAAAATACATCCCGGGCACGAAAATGATC TTCGTGGGCATCAAAAAAAGAAGAACGCG CGGACCTGATCGCGTACCTGAAAAAGGCGAC GAACGAATGA - 3'	<i>Integrated DNA Technologies (IDT)</i>	Custom synthesis, https://eu.idtdna.com/

K86A/K87A/K88A Cc-encoding gBlock: 5' - ATGGGCGACGTGAAAAAGGGCAAAAAGATCT TCATCATGAAATGCTCGCAGTGCCACACGGT GAAAAAGGCGGCAAACACAAAACCGGTCCC AACCTGCACGGCCTGTTTCGGCCGAAAACGG GCCAGGCGCCGGGCTACAGCTACACGGCGG CGAACAAAAACAAAGGCATCATCTGGGGCGA AGACACGCTGATGGAATACCTCGAGAACCCG AAAAAATACATCCCGGGCACGAAAATGATCTT CGTGGGCATCGCCGCCCGCAAGAACGCGC GGACCTGATCGCGTACCTGAAAAAGGCGACG AACGAATGA - 3'	<i>Integrated DNA Technologies (IDT)</i>	Custom synthesis, https://eu.idtdna.com/
K86R/K87R/K88R Cc-encoding gBlock: 5' - ATGGGCGACGTGAAAAAGGGCAAAAAGATCT TCATCATGAAATGCTCGCAGTGCCACACGGT GAAAAAGGCGGCAAACACAAAACCGGTCCC AACCTGCACGGCCTGTTTCGGCCGAAAACGG GCCAGGCGCCGGGCTACAGCTACACGGCGG CGAACAAAAACAAAGGCATCATCTGGGGCGA AGACACGCTGATGGAATACCTCGAGAACCCG AAAAAATACATCCCGGGCACGAAAATGATCTT CGTGGGCATCAGGAGGAGGGAAGAACGCGC GGACCTGATCGCGTACCTGAAAAAGGCGACG AACGAATGA - 3'	<i>Integrated DNA Technologies (IDT)</i>	Custom synthesis, https://eu.idtdna.com/
pET28a(+) expression vector for SET/TAF- β	Martínez-Fábregas <i>et al.</i> (2014) ³²	https://doi.org/10.1074/mcp.M113.034322 .
pET28a(+) expression vector for Q69C SET/TAF- β	This manuscript	N/A
pET28a(+) expression vector for D226C SET/TAF- β	This manuscript	N/A
pET28a(+) expression vector for E243C SET/TAF- β	This manuscript	N/A
pET28a(+) expression vector for D260C SET/TAF- β	This manuscript	N/A
pET28a(+) expression vector for D277C SET/TAF- β	This manuscript	N/A
pET28a(+) expression vector for NPM1	González-Arzola <i>et al.</i> (2022) ³⁴	https://doi.org/10.1038/s41594-022-00842-3
pET14b expression vector for SET/TAF- β Δ C	Muto <i>et al.</i> (2007) ³⁹	https://doi.org/10.1073/pnas.0603762104
pET14b expression vector for Q69C SET/TAF- β Δ C	Casado-Combreras <i>et al.</i> (2022) ⁴⁴	https://doi.org/10.1016/j.csbj.2022.07.009
pBTR1 expression vector (Cc)	Olteanu <i>et al.</i> (2003) ¹⁰⁸	Addgene RRID: Addgene_22468
pBTR1 expression vector for K5A/K7A/K8A Cc	This manuscript	N/A
pBTR1 expression vector for K86R/K87R/K88R Cc	This manuscript	N/A
pLW01 expression vector (Cc)	Pecina <i>et al.</i> (2010) ¹⁰⁹	https://doi.org/10.1021/bi100486s
pLW01 expression vector for K5R/K7R/K8R Cc	This manuscript	N/A
pLW01 expression vector for K86A/K87A/K88A Cc	This manuscript	N/A

Software and algorithms		
Spectra Manager	<i>Jasco</i>	https://jascoinc.com/products/spectroscopy/molecular-spectroscopy-software/
SEQUEST™ HT search engine	<i>Thermo Scientific</i>	https://www.thermo.com/es/es/home/industrial/mass-spectrometry/liquid-chromatography-mass-spectrometry-lc-ms/lc-ms-software/multi-omics-data-analysis/teome-discoverer-software.html
Nano Analyze	<i>TA Instruments</i>	https://www.tainstruments.com/support/software-downloads-support/?lang=es
TopSpin NMR software (version 4.0.6)	<i>Bruker</i>	https://www.bruker.com/en/products-and-solutions/mr/nmr-software/topspin.html
OpenMM	Eastman <i>et al.</i> (2017) ¹¹³	https://openmm.org/
AMBER 16 package	Case <i>et al.</i> (2016) ¹¹⁴	https://ambermd.org
UCSF Chimera 1.15	Pettersen <i>et al.</i> (2004) ¹²⁰	https://www.cgl.ucsf.edu/chimera/
Adaptive Poisson-Boltzmann Solver (APBS, version 3.4.1, web server)	Jurrus <i>et al.</i> (2018) ¹²¹	https://server.poissonboltzmann.org/
PDB2PQR (version 3.6.1, web server)	Dolinsky <i>et al.</i> (2004) ¹²²	https://server.poissonboltzmann.org/
MODELLER	Webb and Sali (2017) ¹⁰⁵	https://salilab.org/modeller/
LAS X	<i>Leica Microsystems</i>	https://www.leica-microsystems.com/products/microscope-software/
LAS-AF	<i>Leica Microsystems</i>	https://www.leica-microsystems.com/products/microscope-software/
FIJI (ImageJ)	Schindelin <i>et al.</i> (2012) ¹²³	https://fiji.sc/
Origin 2018b	<i>OriginLab Corporation</i>	https://www.originlab.com/index.aspx?go=PRODUCTS/Origin
Other		
HisPur™ Ni-NTA resin	<i>Thermo Scientific</i>	Cat. n.: 88222
<i>Foresight Nuvia S</i> 5 mL column	<i>BioRad</i>	Cat. n.: #7324743
3 kDa / 10 kDa cut-off Amicon Ultra™ centrifugal filters	<i>Merck Millipore</i>	Cat. n.: UFC9003 / UFC9010
PD-10 desalting columns	<i>GE Healthcare / Cytiva</i>	Cat. n.: GE17-0851-01